11632 *J. Am. Chem. Soc.* **2000,** *122,* 11632−11648

Spectroscopic and Electronic Structural Studies of Blue Copper Model Complexes. 2. Comparison of Three- and Four-Coordinate Cu(II)−Thiolate Complexes and Fungal Laccase

David W. Randall,[†] Serena DeBeer George,[†] Patrick L. Holland,[‡] Britt Hedman,[†,§] Keith O. Hodgson,[†,§] William B. Tolman,*[,‡] and Edward I. Solomon*[,†]

Contribution from the Department of Chemistry, Stanford University, 333 Campus Drive, Stanford, California 94305, Department of Chemistry and Center for Metals in Biocatalysis, University of Minnesota, 207 Pleasant Street SE, Minneapolis, Minnesota 55455, and Stanford Synchrotron Radiation Laboratory, Stanford Linear Accelerator Center, Stanford University, Stanford, California 94309

Received May 9, 2000

Abstract: To evaluate the importance of the axial ligand in blue Cu centers, the electronic structure of a three-coordinate model compound $LCuSCPh_3$ (**2**, L = β-diketiminate ligand) is defined using low-temperature absorption, magnetic circular dichroism (MCD), X-ray absorption spectroscopy (XAS), and resonance Raman (rR) profiles coupled with density functional calculations. Using these excited-state spectroscopic methods the electronic structure of **2** is compared to that of a four-coordinate blue Cu model compound $LCuSCPh_3$ (**1**, L = tris(pyrazolyl)hydroborate ligand) and the three-coordinate blue Cu center in fungal laccase. The spectral features of **2** are substantially altered from those of **1** and reflect a *trans* influence of the β-diketiminate ligand that involves a strong interaction with the Cu $d_{x^2-y^2}$ orbital, concomitant with a decreased S pπ interaction with the Cu $d_{x^2-y^2}$ orbital. The lack of an axial ligand coupled with the influence of this equatorial donor leads to many of the perturbed spectral features of **2** relative to **1** including: the shift of the S pπ → Cu CT transition to lower energy and its reduced intensity, the stronger ligand field, the larger nitrogen covalency in the HOMO at the expense of thiolate covalency, and the decreased excited-state distortion. From XAS, it also is clear that loss of the axial pyrazole ligand in **2** relative to **1** leads to an increase in the effective nuclear charge of the three-coordinate Cu in **2**, which demonstrates that the axial ligand modulates the electronic structure. From a comparison of **2** to fungal laccase it is evident that even in the absence of an axial ligand the electronic structure can be modulated by differential charge donation from the equatorial ligands. These studies show that elimination of the axial ligand of the blue copper site can affect the covalency of the thiolate−Cu bond and potentially modify the electron-transfer properties of the site.

1. Introduction

Blue Cu proteins[1−4] are important in both intra- and interprotein biological electron transfer (ET).[5−8] The prototypical blue, or type 1, Cu center in plastocyanin, which is important in photosynthesis, is characterized by a trigonally distorted tetrahedral geometry,[9,10] where three strong ligands, $N(His)_2S$-(Cys), form a trigonal plane. The Cu−S(Cys) bond is very short (2.1 Å), while the Cu−N(His) interactions are fairly typical (2.0 Å). The fourth ligand, S(Met), in the ligation sphere of the prototypical blue Cu site is very long (Cu−S ≈ 2.8 Å).[10] Within the diverse array of blue Cu proteins, the strength of this axial ligand interaction shows considerable variability, which provides a possible mechanism for adjusting the properties of the site and thereby influencing reactivity. There are three general classes of axial ligand interactions in blue Cu proteins. The first includes a continuum of tetragonally distorted protein sites where the axial Cu−thioether bond length decreases and is coupled to a weakened Cu−thiolate bond and rotation of the S−Cu−S plane relative to the N−Cu−N plane.[11,12] In the second class, which is typified by stellacyanin, the axial ligand is changed to the stronger O(Gln) ligand, which leads to a tetrahedral distortion of the site.[11,13] In the third class, which is exemplified by the

---

* To whom correspondence should be addressed. Fax: (650) 725-0259. E-mail: Edward.Solomon@stanford.edu.

[†] Department of Chemistry, Stanford University.

[‡] University of Minnesota.

[§] Stanford Synchrotron Radiation Laboratory, Stanford Linear Accelerator Center, Stanford University.

(1) Baker, E. N. In *Encyclopedia of Inorganic Chemistry*; King, R., Ed.; Wiley: Chichester, 1994; pp 883−905.

(2) Adman, E. T. *Adv. Protein Chem.* **1991**, *42*, 145−197.

(3) Sykes, A. G. *Adv. Inorg. Chem.* **1991**, *36*, 377−408.

(4) Solomon, E. I.; Baldwin, M. J.; Lowery, M. D. *Chem. Rev.* **1992**, *92*, 521−542.

(5) Nocek, J. M.; Zhou, J. S.; DeForest, S.; Priyadarshy, S.; Beratan, D. N.; Onuchic, J. N.; Hoffman, B. M. *Chem. Rev.* **1996**, *96*, 2459−2489.

(6) Gray, H. B.; Winkler, J. R. *Annu. Rev. Biochem.* **1996**, *65*, 537−561.

(7) Ullmann, G. M.; Knapp, E. W.; Kostic, N. M. *J. Am. Chem. Soc.* **1997**, *119*, 42−52.

(8) Sigfridsson, K. *Photosyn. Res.* **1998**, *57*, 1−28.

(9) Colman, P. M.; Freeman, H. C.; Guss, J. M.; Murata, M.; Norris, V. A.; Ramshaw, J. A. M.; Venkatappa, M. P. *Nature* **1978**, *272*, 319−324.

(10) Guss, J. M.; Bartunik, H. D.; Freeman, H. C. *Acta Crystallogr.* **1992**, *B48*, 790−811.

(11) LaCroix, L. B.; Randall, D. W.; Nersissian, A. M.; Hoitink, C. W. G.; Canters, G. W.; Valentine, J. S.; Solomon, E. I. *J. Am. Chem. Soc.* **1998**, *120*, 9621−9631.

(12) Randall, D. W.; Gamelin, D. R.; LaCroix, L. B.; Solomon, E. I. *J. Biol. Inorg. Chem.* **2000**, *5*, 16−29.

(13) Hart, P. J.; Nersissian, A. M.; Herrmann, R. G.; Nalbandyan, R. M.; Valentine, J. S.; Eisenberg, D. *Protein Sci.* **1996**, *5*, 2175−2183.

10.1021/ja001592o CCC: $19.00

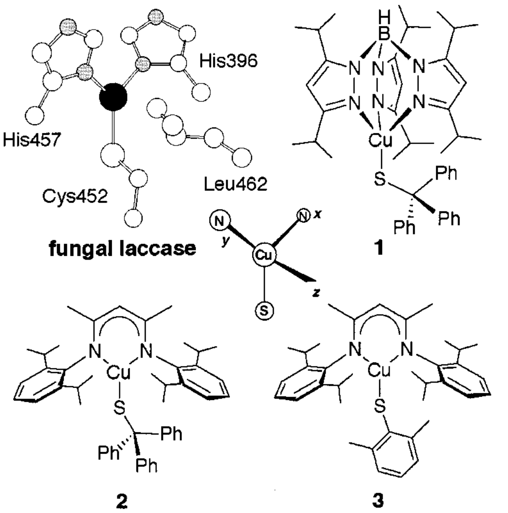

Figure 1. Biological and synthetic Cu(II) thiolates. The blue Cu center in fungal laccase (PDB Code: 1A65). Complex **1**, [HB(pz′)$_3$]CuSCPh$_3$; complex **2**, (β-diketiminate)CuSCPh$_3$; and complex **3**, (β-diketiminate)-CuSC$_6$H$_3$Me$_2$.

type 1 center in fungal laccase, the axial ligand is absent.[14] Thus, the role of the axial ligand in tuning the electronic structure is an important issue for blue Cu centers.[12,15−18]

A small-molecule model complex (**2**) (Figure 1) that has been recently prepared[19] reproduces the uncommon trigonal Cu(II) geometry present in the oxidized fungal laccase type 1 Cu site[14] (Figure 1). Complex **2** incorporates a bidentate β-diketiminate nitrogen ligand with 1.9 Å Cu−N bonds and a triphenylmethylthiolate with a 2.1 Å Cu−thiolate bond,[19] similar to the analogous distances in fungal laccase.[14] Direct comparison of the electronic structures of the trigonal, three-coordinate Cu(II) sites in **2** and fungal laccase is complicated by the fact that the thiolate ligands are different: triphenylmethylthiolate in **2** versus cysteinate in fungal laccase. In the accompanying paper[20] the differences in the electronic structure associated with this change in the thiolate ligand are addressed by comparing the spectroscopically defined electronic structure of the prototypical blue Cu site in plastocyanin[21,22] to that of a tris(pyrazolyl)hydroborate-supported model complex, **1**, that incorporates this thiolate (Figure 1).[23−25] From this study, the ligating S atom in triphenylmethylthiolate is shown to be a stronger donor than the ligating S(Cys) in blue Cu centers. Complex **2** also differs from the trigonal site in fungal laccase in that the β-diketiminate ligand is used, which permits an evaluation of the influence of equatorial ligands other than N(His) (or the closely related N(pz)). To systematically evaluate the change in electronic structure between the blue Cu center and complex **2**, it is important to separate the influences of the thiolate ligand from those of the β-diketiminate nitrogen ligand. Comparing **2** to **1**, which both incorporate the same thiolate ligand, isolates the electronic structural effects of the thiolate ligand from those of the nitrogen ligand and permits an evaluation of the importance of axial ligation.

In this work, a multifaceted, excited-state spectroscopic analysis incorporating absorption, magnetic circular dichroism (MCD), resonance Raman (rR), and X-ray absorption spectroscopy (XAS) methodologies is coupled with density functional theory (DFT) calculations to characterize the electronic structure of **2**. The electronic structure of **2** is compared with the electronic structure of **1** that was defined by parallel studies in the accompanying paper.[20] Absorption and MCD spectroscopies provide a method to distinguish the ligand field transitions from the charge-transfer transitions, which provides insight into changes in the ligand field environment. A vibrational analysis of an isotopically labeled complex, **3** (Figure 1), related to **2** assists in assigning the Raman spectrum. Time-domain analysis of the Raman profile data quantitates the excited-state Cu−S bond length distortion associated with the charge-transfer transition. XAS provides insight into the nature of the ground-state wave function and comparison with **1** provides an estimate of the relative effective nuclear charges (Z_{eff}) of Cu. DFT calculations indicate important factors affecting the copper−thiolate bonding interaction and the importance of the axial ligand Finally, the electronic structure determined from the spectroscopic analysis of **2** is compared to that of the naturally occurring trigonal Cu S(Cys) thiolate center in fungal laccase.

2. Experimental Procedures

2.1. Compounds. Published syntheses of **1**, **2**, and LCuCl (L = β-diketiminate ligand shown in Figure 1) were used.[19,24] All synthetic procedures were performed in an inert-atmosphere glovebox or using standard Schlenk techniques. The sodium salt of 2,6-dimethylphenylthiol was prepared by adding the thiol (1 mL, 7.5 mmol) to a slurry of sodium hydride (455 mg) in THF (20 mL), concentrating to 5 mL, filtering, and precipitating with pentane (10 mL) to yield a white solid consisting of the sodium thiolate and solvated THF (~0.5 equiv by ^{1}H NMR spectroscopy).

2.1.1. Preparation of 3. A solution of NaSC$_6$H$_3$(CH$_3$)$_2\cdot{}^1/_2$THF (25 mg, 0.13 mmol) in THF (3 mL) was added slowly to a red−purple slurry of LCuCl (66 mg, 0.13 mmol) in THF (10 mL). The resultant deep blue solution was stirred for 30 min and then slowly dried in vacuo. The residue was extracted with pentane (10 mL), filtered through a plug of Celite, and concentrated to 5 mL. This solution was cooled overnight to give crystals of **2** (20 mg, 25% yield). UV−vis (pentane) [$\lambda_{\max}$, nm (ϵ, mM^{-1} cm^{-1})]: 340 (~29), 458 (2.1), 729 (6.4); EPR (9.61 GHz, toluene, 20 K): $g_{\parallel} = 2.18$, $A_{\parallel} = 115 \times 10^{-4}$ cm^{-1}, $g_{\perp} = 2.04$, $A_{\perp} = 13 \times 10^{-4}$ cm^{-1} (simulated with QPOWA[26]); Anal. Calcd for C$_{48}$H$_{56}$CuSN$_2$: C, 71.86; H, 8.15; N, 4.53. Found: C, 71.80; H, 8.30; N, 4.58. The X-ray crystal structure of **3** is presented in the Supporting Information. Important crystallographic data: monoclinic, space group $P2_1/c$, $a = 11.3523(2)$ Å, $b = 17.0133(3)$ Å, $c = 18.3511(2)$ Å, $\beta = 103.490(1)°$, $V = 3446.55(9)$ Å^3, $Z = 4$, $\rho_{\mathrm{calcd}} = 1.192$ g/cm^3. Non-hydrogen atoms were refined with anisotropic thermal parameters, and

---

(14) Ducros, V.; Brzozowski, A. M.; Wilson, K. S.; Brown, S. H.; Ostergaard, P.; Schneider, P.; Yaver, D. S.; Pedersen, A. H.; Davies, G. J. *Nat. Struct. Biol.* **1998**, *5*, 310−316.

(15) Palmer, A. E.; Randall, D. W.; Xu, F.; Solomon, E. I. *J. Am. Chem. Soc.* **1999**, *121*, 7138−7149.

(16) Xu, F.; Berka, R. M.; Wahleithner, J. A.; Nelson, B. A.; Shuster, J. R.; Brown, S. H.; Palmer, A. E.; Solomon, E. I. *Biochem. J.* **1998**, *334*, 63−70.

(17) Lowery, M. D.; Solomon, E. I. *Inorg. Chim. Acta* **1992**, *200*, 233−243.

(18) Olsson, M. H. M.; Ryde, U. *J. Biol. Inorg. Chem.* **1999**, *4*, 654−663.

(19) Holland, P. L.; Tolman, W. B. *J. Am. Chem. Soc.* **1999**, *121*, 7270−7271.

(20) Randall, D. W.; George, S. D.; Hedman, B.; Hodgson, K. O.; Fujisawa, K.; Solomon, E. I. *J. Am. Chem. Soc.* **2000**, *122*, 11620−11631.

(21) Gewirth, A. A.; Solomon, E. I. *J. Am. Chem. Soc.* **1988**, *110*, 3811−3819.

(22) LaCroix, L. B.; Shadle, S. E.; Wang, Y. N.; Averill, B. A.; Hedman, B.; Hodgson, K. O.; Solomon, E. I. *J. Am. Chem. Soc.* **1996**, *118*, 7755−7768.

(23) Kitajima, N.; Fujisawa, K.; Moro-oka, Y. *J. Am. Chem. Soc.* **1990**, *112*, 3210−3212.

(24) Kitajima, N.; Fujisawa, K.; Tanaka, M.; Moro-oka, Y. *J. Am. Chem. Soc.* **1992**, *114*, 9232−9233.

(25) Qiu, D.; Kilpatrick, L. T.; Kitajima, N.; Spiro, T. G. *J. Am. Chem. Soc.* **1994**, *116*, 2585−2590.

(26) (a) M. J. Nilges, Ph.D. Thesis, University of Illinois, Urbana, Illinois, 1979. (b) Belford, R. L.; Nilges, M. J. "Computer Simulation of Powder Spectra", EPR Symposium, 21st Rocky Mountain Conference, Denver, Colorado, August, 1979. (c) A. M. Maurice, Ph.D. Thesis, University of Illinois, Urbana, Illinois, 1980.

hydrogen atoms were in idealized positions with riding thermal parameters. Full-matrix least squares refinement on F^2 converged with $R1 = 0.0295$, $wR^2 = 0.0727$, GOF = 1.033 for 4760 independent reflections ($I > 2\sigma(I)$) and 382 parameters.

2.1.2. Sulfur-34 Labeling. Preparation of ^{34}S-enriched 2,6-dimethylphenylthiol was accomplished by addition of solid sulfur-34 (45 mg, 1.3 mmol, 77% atomic enrichment, Cambridge Isotopes) to a solution of 2,6-dimethylphenyl magnesium bromide (1.0 mL, 1.0 M in THF, Aldrich) at room temperature. This solution was stirred under nitrogen for 3 h, and then lithium aluminum hydride (~0.1 g) was added, causing the pale yellow color to fade. The reaction was quenched with saturated NH_4Cl (50 mL), and the aqueous layer was extracted with three portions of 25 mL of diethyl ether. The combined organic layers were dried over $MgSO_4$, reduced to an oil, and distilled at 45 °C (0.1 mmHg) to yield a sample of labeled 2,6-dimethylphenylthiol that was used to make the sodium salt (as described above) without further manipulation. Synthesis of isotopically labeled complex **3** was accomplished using procedures similar to those described above.

2.2. UV−Vis Absorption and MCD. Room-temperature absorption spectra were recorded in heptane, pentane, or toluene on a HP8453 diode-array spectrophotometer. Low-temperature UV−vis absorption spectra were recorded at ~10 K using either a Cary 500 or Cary 17 equipped with a Janis Supervaritemp dewar. MCD spectra were recorded using Jasco J500 (or J810, UV−visible, PMT detection) and J200 (near-IR, liquid nitrogen-cooled InSb solid-state detection) spectropolarimeters modified to include Oxford SM-4 (7 T, UV−vis) or SM-4000 (7 T, near-IR) superconducting magnets with optical access within their sample compartments. Special care was taken to provide magnetic shielding for the PMT detector. For low temperature MCD experiments, solid samples (mulls) that were prepared by finely grinding microcrystalline material into powders with a mortar and pestle and then adding mulling agents (poly(dimethylsiloxane) (Aldrich) or Fluorolube (Wilmad)) were uniformly spread between quartz disks (Heraeus-Amersil) and loaded into copper MCD cells and promptly frozen in liquid nitrogen.

2.4. Raman and Resonance Raman Enhancement Profiles. In initial rR spectra and sulfur-34 labeling experiments performed at Minnesota, resonance Raman spectra were collected on an Acton 506 spectrometer using a Princeton Instruments LN_2/CCD-1100-PB/UVAR detector and ST-1385 controller, equipped with a 1200 grooves/mm holographic grating, interfaced with Winspec software. A grating with 2400 grooves/mm was used for confirmation of the small ^{34}S isotope shifts, and the shifts reported here are deemed accurate to 1 cm^{-1}. A Spectra-Physics 2030-15 Ar ion laser at a power of 4 W was employed to pump a 375B CW dye (Rhodamine 6G) laser at 632.8 nm. Solutions (~50 mM, d_6-benzene) were frozen onto a gold-plated copper coldfinger in thermal contact with a dewar containing liquid nitrogen. The spectra were obtained at 77 K using a 135° backscattering geometry. Raman shifts were referenced externally through a quadratic fit to the known spectrum of indene at room temperature.[27]

At Stanford, (resonance) Raman spectra were recorded using a Princeton Instruments, liquid nitrogen cooled, back-illuminated CCD camera mounted on a Spex 1877 0.6 m triple spectrometer, equipped with 1200, 1800, or 2400 grooves/mm holographic gratings. Continuous wave Coherent Kr ion (Innova 90C-K) and Ar ion (Sabre-25/7) visible and UV laser lines were used for variable-energy excitation. A polarization scrambler was placed in front of the entrance slits of the spectrometer. Samples were loaded in 5-mm (o.d.) NMR tubes immersed in liquid nitrogen, and spectra were obtained in a ~135° backscattering geometry with ~40 mW incident power. Raman scattering resolution and accuracy is ~2 cm^{-1}. Raman peak profile intensities were determined relative to normal Raman scattering of solvent peaks. Resonance Raman enhancement profiles (RREPs) were simulated using the time-dependent theory of Heller, et al.[28−32] that was implemented in a MathCAD script.[33] The parameters of the fits were adjusted until the simulated spectra reasonably matched the experimental data. The same set of parameters was used to simulate both the resonance Raman enhancement profile and the absorption spectrum.

2.5. X-ray Absorption Spectroscopy Measurements and Data Analysis. All data were measured at the Stanford Synchrotron Radiation Laboratory under ring conditions 3.0 GeV and 60−100 mA.

S K-edge data were measured using the 54-pole wiggler beam line 6-2 in high magnetic field mode of 10 kG with a Ni-coated harmonic rejection mirror and fully tuned Si(111) double crystal monochromator. Details of the optimization of this setup for low-energy studies have been described in an earlier publication.[34] S K-edge measurements were made at room temperature. Samples were ground into a fine powder and dispersed as thinly as possible on Mylar tape to minimize the possibility of self-absorption. The data were measured as fluorescence excitation spectra utilizing an ionization chamber as a fluorescence detector.[35,36] To check for reproducibility, 2−3 scans were measured for each solid sample. The energy was calibrated from S K-edge spectra of $Na_2S_2O_3{\cdot}5H_2O$, run at intervals between sample scans. The maximum of the first preedge feature in the spectrum was assigned to 2472.02 eV. Data were averaged, and a smooth background was removed from all spectra by fitting a polynomial to the preedge region and subtracting this polynomial from the entire spectrum. Normalization of the data was accomplished by fitting a flattened polynomial or straight line to the postedge region and normalizing the edge jump to 1.0 at 2490 eV. Fits to the edges were performed using the program EDG_FIT.[37] Second derivative spectra were used as guides to determine the number and position of peaks. Preedge and rising edge features were modeled by pseudo-Voigt line shapes. For the preedge feature, a fixed 1:1 ratio of Lorentzian to Gaussian contributions was used. Fits were performed over several energy ranges. The reported intensity values and standard deviations are based on the average of all good fits. Normalization procedures can introduce ~3% error in preedge peak intensities, in addition to the error resulting from the fitting procedure.

Cu L-edge data were measured using the 31-pole wiggler beam line 10-1. Samples were finely ground and spread across double-adhesive conductive carbon tape, which was attached to an aluminum paddle. The data were measured at room temperature as total electron yield spectra utilizing a Galileo 4716 channeltron electron multiplier as a detector. For each sample, 3−4 scans were measured to check reproducibility. The energy was calibrated from the Cu L-edge spectra of CuF_2, run at intervals between sample scans. The maximum of the L_3 and L_2 preedges were assigned to 930.5 and 950.5 eV, respectively. A linear background was fit to the preedge region (870−920 eV) and was subtracted from the entire spectrum. Normalization was accomplished by fitting a straight line to the postedge region and normalizing the edge jump to 1.0 at 1000 eV. Fits to the edges were performed using EDG_FIT.[37] A pseudo-Voigt peak was used to model the L_3 and L_2 2p → 3d transitions. Arctangent functions were used to model the L_3 and L_2 edge jumps. The total L-preedge intensity reported here was calculated as $L_3 + L_2$. The reported intensity values and standard deviations are based on the average of all good fits. Normalization procedures can introduce ~4% error in preedge peak intensities, in addition to the error resulting from the fitting procedure.

2.6. Calculations. Density functional theory (DFT) calculations were performed using the Amsterdam Density Functional package of Baerends and co-workers (ADF 2.0.1) using the database IV basis set.[38,39] The Vosko, Wilk, Nusair local density approximation[40] was used for exchange and correlation, respectively. Generalized gradient

---

[27] *Methods in Enzymology*; Riordan, J. F.; Vallee, B. L., Eds.; Academic Press: New York, 1993; Vol. 226, p 351.

[28] Heller, E. J. *Acc. Chem. Res.* **1981**, *14*, 368−375.

[29] Heller, E. J.; Sundberg, R. L.; Tannor, D. *J. Phys. Chem.* **1982**, *86*, 1822−1833.

[30] Myers, A. B.; Mathies, R. A. In *Biological Applications of Raman Spectroscopy*; Spiro, T. G., Ed.; Wiley: New York, 1987; Vol. 2, pp 1−58.

[31] Myers, A. B. *Acc. Chem. Res.* **1997**, *30*, 519−527.

[32] Zink, J. I.; Shin, K. S. K. *Adv. Photochem.* **1991**, *16*, 119−214.

[33] Brunold, T. C.; Tamura, N.; Kitajima, N.; Moro-oka, Y.; Solomon, E. I. *J. Am. Chem. Soc.* **1998**, *120*, 5674−5690.

[34] Hedman, B.; Frank, P.; Gheller, S. F.; Roe, A. L.; Newton, W. E.; Hodgson, K. O. *J. Am. Chem. Soc.* **1988**, *110*, 3798−3805.

[35] Stern, E. A.; Heald, S. M. *Rev. Sci. Instrum.* **1979**, *50*, 1579−1582.

[36] Lytle, F. W.; Greegor, R. B.; Sandstrom, D. R.; Marques, E. C.; Wong, J.; Spiro, C. L.; Huffman, G. P.; Huggins, F. E. *Nucl. Instrum. Methods* **1984**, *226*, 542−548.

[37] George, G. N. EDG_FIT; Stanford Synchrotron Radiation Laboratory, Stanford Linear Accelerator Center, Stanford University, Stanford, CA 94309.

approximations of Becke[41] and Perdew[42] were included for exchange and correlation. The calculations reported here are for spin-restricted systems; however, spin-unrestricted calculations gave very similar results. Calculations were also attempted with the Gaussian 98 package using the B3LYP functional[43] and the SCF-Xα-SW package.[44] However, these packages give a ground electronic state that is inconsistent with experiment; a β-diketiminate ligand-based HOMO ($\pi_{nb,b1}$ in Table 5) is calculated, rather than a Cu-based HOMO. For the B3LYP calculations, several basis sets, including many with different degrees of polarization, all gave the $\pi_{nb,b1}$ ground state. To model the geometry of **2**, only the essential $C_3H_5N_2^-$ core of the β-diketiminate ligand was retained. Likewise, the thiolate was approximated by SCH_3^-. The calculations on the resulting $[C_3H_5N_2CuSCH_3]^0$ complex were done single point at the X-ray structure, but symmetrized to C_s. Thus, the small deviation of the Cu from the N_2S plane was retained. Input files, including the atomic coordinates, are included in the Supporting Information.

3. Results and Analysis

3.1. Synthesis and Characterization of a 3-Coordinate Aryl Thiolate Complex. Using synthetic methods analogous to those used for **2**,[19] a 3-coordinate β-diketiminate Cu(II) complex of the 2,6-dimethylphenylthiolate ligand was prepared. The X-ray crystal structure of this product, **3**, is presented in the Supporting Information. The geometry of **3** is very similar to that of **2**, with the copper atom lying only 0.1046(7) Å from the N_2S plane, demonstrating its trigonal coordination sphere. Most notable are the small differences in bond angles and lengths, some of which are attributable to the lesser steric demands of the aryl group versus the triphenylmethyl group. For example, the Cu−S−C angle is substantially smaller (107.63(7)° in **3** versus 119.43(8)° in **2**), and the S−C (1.789(2) Å in **3** versus 1.883(2) Å in **2**) and Cu−N (average 1.902 Å in **3** vs 1.922 Å in **2**) bonds are shorter. Interestingly, though, the Cu−S bond is longer (2.1382(5) in **3** vs 2.1243(8) in **2**), pointing to a "push−pull" effect between the thiolate and the β-diketiminate ligand; this theme will be elaborated at length below.

Despite these structural modifications, the substitution of an aryl group in **3** for the alkyl group of **2** causes only minimal changes in the electronic absorption and EPR spectra. Thus the intense low-energy charge-transfer absorption (vide infra) lies at 729 nm in **3** (749 nm in **2**), and the EPR spectrum of **3** is nearly superimposable on that of **2**. Because of these similarities, compound **3** will be discussed below only in the context of resonance Raman spectroscopy, where it was possible to use the ^{34}S-labeled form of **3** to identify vibrations involving Cu−S stretching.

3.2. Absorption and Magnetic Circular Dichroism Spectroscopy.

3.2.1. Absorption. As demonstrated in Figure 2A and summarized in Table 1, the absorption spectrum of **2** is characterized by an intense, low-energy transition at ~750 nm (= 13500 cm^{-1}; $\epsilon \approx 5400$ M^{-1} cm^{-1}) (band 3).[19] Between 15000 and 25000 cm^{-1} there are several weaker bands (bands 4−8, $\epsilon < 1200$ M^{-1} cm^{-1}). At 28500 cm^{-1} lies intense ($\epsilon \approx$ 16400 M^{-1} cm^{-1}) band 9. Gaussian fits that are simultaneously consistent with both the absorption spectrum and the low-temperature MCD spectrum (vide infra) are included in the figure and summarized in Table 1. The low-temperature mull absorption spectrum (not shown) is similar in general appearance to that shown in Figure 2A.

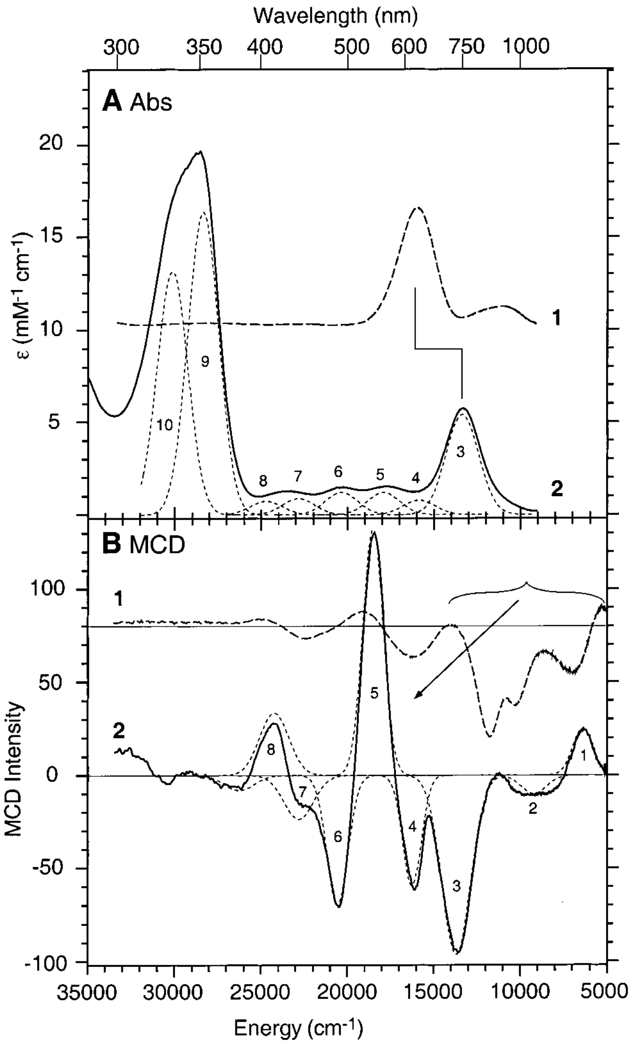

Figure 2. Excited-state electronic spectra of complex **2**, (β-diketiminate)$CuSCPh_3$ in heptane in comparison to complex **1**, $[HB(pz')_3]$-$CuSCPh_3$. (A) Room-temperature absorption spectrum of **2**, including an overlay of Gaussian fits summarized in Table 1. (B) Low-temperature (5 K) magnetic circular dichroism (MCD) spectrum of **2** at a field of 7 T, including Gaussian fits summarized in Table 1.

Table 1. Experimental MCD and Absorption Band Characterization for **2**

band	assignment	energy (cm^{-1})	ϵ (M^{-1} cm^{-1})	osc str	MCD/ABS[a]
1	d_{z^2}	6300	−	nd	+ve
2	$\pi_{nb,b1}$	~9000	−	nd	−ve
3	S pπ CT	13500	5400	0.0553	−0.018
4	d_{xy}	16100	780	0.0081	−0.075
5	d_{yz+xz}	18200	1200	0.0123	+0.110
6	d_{yz-xz}	20450	1210	0.0124	−0.057
7	S p ps.σ	22800	880	0.0090	−0.027
8	π_{a2}	24700	740	0.0076	+0.045
9	Lig $\pi \rightarrow \pi^*$	28500	16360	0.1009	nd

[a] Ratio of MCD intensity to absorption intensity. This ratio approximates the relative C/D ratios for mull data, where it is impossible to obtain absolute C/D ratios.

3.2.2. MCD. The low-temperature MCD spectrum of a poly(dimethylsiloxane) mull of **2** is presented in Figure 2B. Fits to the spectrum are summarized in Table 1. At the low temperatures employed in these experiments, the MCD intensity originates exclusively from a C-term mechanism as determined

---

(38) ADF 2.0.1; Vrije Universiteit, Theoretical Chemistry, De Boelelaan 1083, 1081 HV Amsterdam, The Netherlands, 1995.

(39) te Velde, G.; Baerends, E. J. *J. Comput. Phys.* **1992**, *99*, 84−98.

(40) Vosko, S. H.; Wilk, L.; Nusair, M. *Can. J. Phys.* **1980**, *58*, 1200−1211.

(41) Becke, A. D. *Phys. Rev. A* **1988**, *38*, 3098−3100.

(42) Perdew, J. P. *Phys. Rev. B* **1986**, *33*, 8822−8824.

(43) Becke, A. D. *J. Chem. Phys.* **1993**, *98*, 5648−5652.

(44) Cook, M.; Case, D. A. *QCPE Program #465*, 1991; Vol. 23.

from the temperature dependence of the MCD spectral intensity; that is, $C \propto (\beta B/kT)\,\Delta\epsilon$, where β is the Bohr magneton, B is the magnetic field, k is the Boltzmann constant, T is the temperature (K), and $\Delta\epsilon$ is the molar circular dichroism. The saturation behavior of the features in the low-temperature MCD spectra gives a g_{iso} value of 2.10, consistent with EPR,[19] though the latter technique better resolves the anisotropy of the g-interaction. A moderately intense MCD band (Figure 2B, band 1) is observed at low energy, 6300 cm^{-1}. Band 2 is observed at ~9000 cm^{-1}. An MCD feature (band 3) is observed at the same energy as the strong 750 nm absorption (13500 cm^{-1}). Of particular importance are the three intense MCD bands (bands 4−6) to *higher* energy than the 750 nm absorption (band 3). In the spectrum shown in Figure 2B, the MCD features in the 28000−30000 cm^{-1} region (bands 9 and above) are distorted due to the strong absorptions in this region. However, a spectrum obtained on a more dilute mull, where this issue is alleviated, does not show significant MCD intensity in this region (not shown).

3.2.3. Band Assignments. The bands in **2** can be assigned in analogy with those in **1**, corresponding spectra for which are included in Figure 2 for comparison,[20] and the blue Cu center in plastocyanin (the coordinate system is given in Figure 1, where z is perpendicular to the S(thiolate)N_2 plane and x and y are bisected by the S(thiolate)−Cu bond).[21,22] For a system like **2**, MCD intensity derives from out-of-state spin−orbit coupling to energetically nearby states. The magnitude of such spin−orbit coupling scales with the spin−orbit coupling constant ξ, which is much larger for Cu (830 cm^{-1}) than for S (380 cm^{-1}) or N (70 cm^{-1}). This enables the use of MCD C-term band intensities relative to absorption band intensities (i.e., C_0/D_0 ratios) to distinguish d → d (or ligand field) transitions, which have strong MCD intensity, from charge-transfer (CT) transitions, which have weaker MCD intensity.[21] The large MCD intensity of bands 4−6 that are clustered around 18500 cm^{-1} in Figure 2B, coupled with their low absorption intensity from Figure 2A (the MCD/Abs ratio, Table 1, for these bands is ~4 times larger than for band 3), enables us to assign these bands as d−d bands. Likewise, the low-energy band 1 is assigned as the fourth d−d band. The specific LF bands are assigned in analogy with those in **1**[20] and the blue Cu center in plastocyanin.[21,22] The signs of the d → d MCD features in **2** are identical to those in plastocyanin.[21] At lowest energy is Cu d_{z^2} (band 1, positive), while Cu d_{xy} (band 4, negative), Cu d_{yz-xz} (band 5, positive), and Cu d_{yz+xz} (band 6, negative), in order of increasing transition energy, lie to higher energy than band 3.

The significant absorption intensity of band 3, the smaller MCD/Abs ratio (0.02, Table 1) than bands 4−6 (0.08 ± 0.03), Raman profile data (vide infra), and density functional calculations (vide infra) indicate that this low-energy, intense transition is the S pπ → Cu CT transition. Band 2 is associated with the β-diketiminate ligand and will be considered later, as will the assignment of the weak bands 7 and 8. Possibilities for the latter set include N → Cu CT and the S (pseudo-σ) → Cu CT transitions. High energy, intense band 9 is associated with the β-diketiminate N-donor ligand, since the absorption spectrum of spectroscopically transparent lithium, thallium(I), and copper(I) β-diketiminates also show an intense absorption near 350 nm, suggesting that this absorption is general to complexes containing the β-diketiminate ligand.[45] The lack of significant MCD intensity in band 9 further supports the ligand-based assignment for this band, as the C-term MCD intensity will scale with the small ξ values of N and C, relative to Cu. Based on Raman data (vide infra) band 9 is assigned as an intraligand $\pi \rightarrow \pi^*$ transition.

Table 2. Oscillator Strengths for S pπ → Cu CT Band

compound	1	2
osc. strength f_{exp}	0.0777[a]	0.0553[a]
S pπ → Cu CT transition freq/cm^{-1}	16000	13500
freq. scaled $f_{\mathrm{exp,\,sc}}$	0.0777	0.0664

[a] From room-temperature absorption spectra.

3.2.4. Comparison to 1. Many features in the optical spectra of **2** that are presented in Figure 2 are different than those of **1**,[20] in particular, and those of other highly covalent Cu−thiolate centers.[11,15,21,22] As Figure 2A indicates, relative to complex **1**, the intense, low-energy S pπ → Cu CT band (band 3) is shifted to even lower energy in **2**: from 16000 cm^{-1} (625 nm) in **1** to 13500 cm^{-1} (750 nm) in **2**. The energy shift of the CT band is also clear from the MCD spectrum (Figure 2B). The ligand field bands in **2**, which are intense in MCD but weak in absorption, are analogous to the ligand field bands at lower energy than the intense 600 nm band in **1**. However, there is a striking difference in the energies of these ligand field bands between **2** and **1**. Figure 2B demonstrates that bands 4, 5, and 6, which move in concert, are to *much* higher energy in **2** relative to **1**, for example, the highest energy d−d band moves from 11080 cm^{-1} in **1** to 20450 cm^{-1} in **2**. This substantial shift of the d−d bands to higher energy clearly indicates that the ligand field is much stronger in **2**. The low-energy band (band 1) in **2** is analogous to the 5200 cm^{-1} band in **1**, though it is shifted to significantly higher energy (~1100 cm^{-1}). This band corresponds to a transition from the d_{z^2} orbital, which is lower in energy in **2** due to the absence of an axial ligand. This decreases the antibonding interaction along the z-axis and allows the 4s/d_{z^2} mixing to increase. Finally, there are no counterparts in complex **1** for band 2 at ~9000 cm^{-1} and band 9 at 28500 cm^{-1}, confirming their association with the β-diketiminate donor ligand.

Comparison of the intensities of the low energy S pπ → Cu CT bands in **1** and **2** (Figure 2A) reveals a further difference between **1** and **2**. Quantitatively, the band intensity can be expressed by its oscillator strength, f. To determine the oscillator strengths from the experimental data we use the approximation: $f_{\mathrm{exp}} = 4.61 \times 10^{-9}\,\epsilon_{\mathrm{max}}\,\nu_{1/2}$, where ϵ_{max} is the maximum absorption and $\nu_{1/2}$ is the full-width at half-maximum of the peak. The experimental oscillator strengths are 0.077 and 0.055 for **1** and **2**, respectively (see Table 2). Oscillator strengths give a measure of the transition moment[46] ($f(\nu) \propto \nu\cdot|\langle\psi_i|\mu|\psi_f\rangle|^2$) and have an intrinsic ν dependence (i.e., for a constant transition moment the transition intensity f increases with transition energy). Even when the oscillator strength of **2** is scaled by the ratio of the transition frequencies to take this factor into account, the resulting transition moment of **2** is only 86% that of **1** (Table 2). Since absorption intensity is proportional to overlap of the ligand orbitals in the donor and acceptor orbitals involved in the electronic transition, the reduced oscillator strength of **2** compared to **1** points to less S pπ ligand character in the ground-state wave function (i.e., HOMO) of **2**.

3.3. Resonance Raman Spectroscopy.

3.3.1. Vibrations and Isotopic Substitution. Raman spectra of **1**[25] and **2**[19] have been reported previously. Figure 3A compares the resonance Raman (rR) spectra of **2** and **3** using laser excitation into their 750 nm absorption bands and the rR spectrum of **1** obtained using excitation into its 625 nm absorption band. When excited into their S pπ-Cu CT bands,

---

(45) Holland, P. L.; Tolman, W. B. Unpublished work.

(46) Solomon, E. I. *Comm. Inorg. Chem.* **1984**, *3*, 225−320.

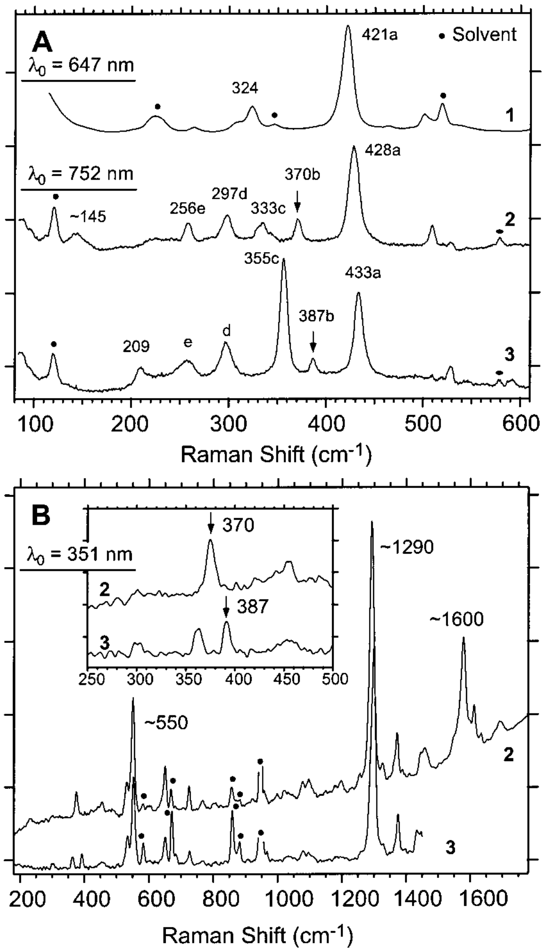

Figure 3. Resonance Raman spectra of Cu(II) thiolate model systems **1** [HB(pz′)$_3$]CuSCPh$_3$, **2** LCuSCPh$_3$, and **3** LCuSC$_6$H$_3$Me$_2$, where L = *β*-diketiminate. (*A*) rR spectra obtained using excitation (λ_0 = 752 nm, 647 nm) into the respective S pπ → Cu CT transitions. The vibration at ~425 cm^{-1} corresponds to the Cu−S stretch, while vertical arrows highlight the Cu−N vibration. Analogous vibrations in **1**, **2**, and **3** are indicated by a, b, c, d, and e, as described in the text. (*B*) rR spectra obtained using excitation (λ_0 = 351 nm) into the high energy π−π* transition. Black dots represent solvent vibrations; **2** and **3** in frozen (77 K) *d*$_6$-benzene and **1** in frozen (~120 K) toluene.

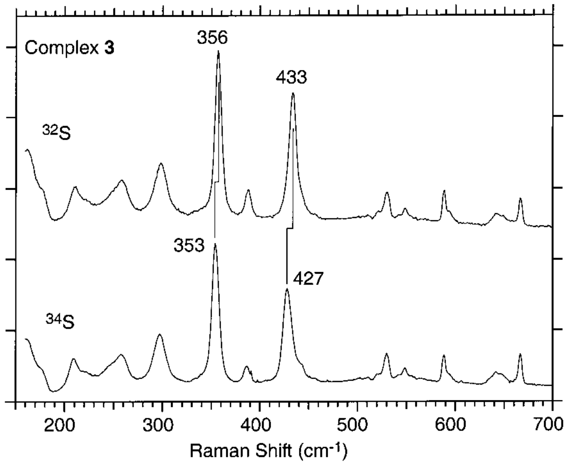

Figure 4. Raman spectrum of **3** in frozen (77 K) *d*$_6$-benzene showing the effect of ^{34}S isotopic labeling; λ_0 = 632.8 nm.

all complexes show an intense band at ~425 cm^{-1}. In complex **1** this band is at 421 cm^{-1}, while in **2** it shifts to 428 cm^{-1} and in **3** it is slightly higher still at 433 cm^{-1} (bands a, Figure 3A). The band at 333 cm^{-1} in **2** appears to shift to 355 cm^{-1} in **3** and become more intense (bands c), while weaker bands at 256 and 297 cm^{-1} (bands d and e) are at essentially identical frequencies in these two complexes. An apparent counterpart to the 333 cm^{-1} band in **2** is observed in complex **1** at 324 cm^{-1}. Further, in the *β*-diketiminate-ligated complexes, a band at 370 cm^{-1} in **2** shifts to 387 cm^{-1} in **3** (bands b). There is an additional band at 209 cm^{-1} in **3** not present in **2**; reciprocally, a band at ~145 cm^{-1} in **2** does not appear to have a counterpart in **3**. To higher Raman shift at this excitation energy (752 nm), the most intense bands are combinations and overtones of the fundamentals (not shown). For complex **3**, which has two intense bands in the 300−450 cm^{-1} region (355 and 433 cm^{-1}), the 2 ν_i overtone for the 433 cm^{-1} band is 5.2 times more intense than the analogous overtone for the 355 cm^{-1} band. The effect of ^{34}S isotopic substitution in **3** on the vibrational spectrum is presented in Figure 4. The most obvious change in the rR spectrum is a 6 cm^{-1} shift in the ~433 cm^{-1} band. A smaller shift of 3 cm^{-1} is also observed for the 355 cm^{-1} band (shifts of other bands are 1 cm^{-1} or less, see Table S1, Supporting Information).

3.3.2. Assignments and Correlations with 1. The fact that the ~425 cm^{-1} vibrational band in all the complexes shows such large enhancement upon excitation into their respective S pπ-Cu CT bands suggests that this vibration be assigned as the Cu−S stretch. The isotopically labeled Raman data in Figure 4 make this assignment unambiguously clear, since ^{34}S incorporation in **3** results in a 6 cm^{-1} shift of the 433 cm^{-1} peak to lower frequency. This assignment parallels and confirms the assignment of Spiro, et al. for **1** (and related complexes)[25] and also the general assignment for blue Cu proteins.[47−50] The model complexes studied here exhibit much less mechanical coupling between the Cu−S stretch and thiolate side chain deformations than in blue Cu proteins, in which this coupling yields their characteristic vibrational envelope in the 350−450 cm^{-1} region.[47−50] In addition to the intense 433 cm^{-1} band, in **3** there is also an intense band at 355 cm^{-1}. However, the substantial enhancement of the 433 cm^{-1} overtone relative to the 355 cm^{-1} overtone and combination bands, suggests that for complex **3**, the 433 cm^{-1} peak is a fairly pure Cu−S stretch. Raman spectra of complexes **2** and **3** are rather similar to those of **1**. In particular, the Cu−S stretching frequency in all of these Cu(II)-thiolate compounds is quite similar and relatively high at ~425 cm^{-1}. This indicates that **1**, **2**, and **3** have Cu−S bonds with similar strengths, independent of the nitrogen ligand. The small difference (7 cm^{-1}) between the Cu−S stretching frequencies in **1** and **2** is consistent with small differences in the Cu−S bond length:[51] 2.12 Å in **2** versus 2.13 Å in **1**.

The 333 cm^{-1} band in **2** that upshifts to 355 cm^{-1} in **3** seems to be analogous to a band in **1** at 322 cm^{-1}. In **3**, the only blue Cu model complex where the thiolate sulfur has been labeled, this band shows a small (3 cm^{-1}) ^{34}S isotope shift relative to the 6 cm^{-1} ^{34}S isotope shift of the 433 cm^{-1} band. A Raman

---

(47) Blair, D. F.; Campbell, G. W.; Schoonover, J. R.; Chan, S. I.; Gray, H. B.; Malmström, B. G.; Pecht, I.; Swanson, B. I.; Woodruff, W. H.; Cho, W. K.; English, A. M.; Fry, H. A.; Lum, V.; Norton, K. A. *J. Am. Chem. Soc.* **1985**, *107*, 5755−5766.

(48) Andrew, C. R.; Sanders-Loehr, J. *Acc. Chem. Res.* **1996**, *29*, 365−372.

(49) Qiu, D.; Dong, S. L.; Ybe, J. A.; Hecht, M. H.; Spiro, T. G. *J. Am. Chem. Soc.* **1995**, *117*, 6443−6446.

(50) Czernuszewicz, R. S.; Dave, B. C.; Germanas, G. P. In *Spectroscopic Methods in Bioinorganic Chemistry*; Solomon, E. I., Hodgson, K. O., Eds.; American Chemical Society: Washington, DC, 1998; pp 220−240.

(51) Herschbach, D. R.; Laurie, V. W. *J. Chem. Phys.* **1961**, *35*, 458−463.

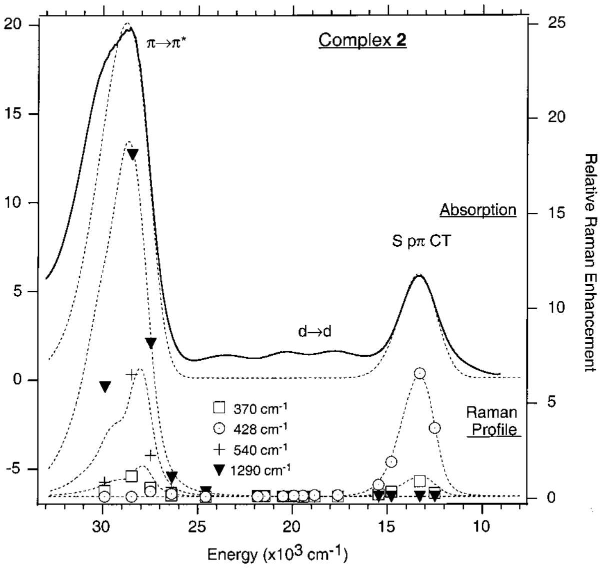

Figure 5. Heller fits of the absorption and resonance Raman enhancement profiles (RREP) for complex **2** using the parameters in the text and summarized in Table 3 for the S p$\pi \rightarrow$ Cu CT band.

spectrum on an aryl thiolate analogue of **1**, [HB(pz′)$_3$]CuSC$_6$F$_5$, (Figure S1, Supporting Information) shows increased intensity in two partially resolved features at ∼340 cm^{-1} and ∼350 cm^{-1}, in parallel to the higher frequency and intensity of the 355 cm^{-1} band in the aryl thiolate complex, **3**, (where R = 2,6-dimethylphenyl) relative to the alkyl thiolate **2** (where R = triphenylmethyl). Given these spectroscopic observations, it appears that in copper−thiolate systems utilizing an aryl thiolate, this vibration(s) is at ∼20 cm^{-1} higher frequency and higher in intensity than with an alkyl thiolate, independent of the nitrogen ligand. This band is likely associated with a limited amount of mechanical coupling of the Cu−S stretch with an internal aryl thiolate ligand vibration involving S.

The excitation wavelength dependence of the Raman spectrum also aids in assigning the Raman spectra. Confirming that they are indeed analogous, the 370 cm^{-1} band in **2** (Figure 5) and the 386 cm^{-1} band in **3** (Figure S2) exhibit very similar Raman enhancement profiles. Figures 5 and S2 demonstrate that these vibrational bands show enhancement both in the low energy (750 nm) CT absorption band as well as the higher energy (350 nm) absorption. This observation is consistent with the assignment of these vibrations as Cu−N stretches. The HOMO of **2** has substantial N character, and therefore, some distortion of the nitrogen ligands would be expected in the low energy S p$\pi \rightarrow$ Cu CT excited state (vide infra). The increase in Cu−N frequency in **3** relative to **2** is consistent with the shorter Cu−N distances (0.02 Å shorter) in the former. Complex **1** does not appear to have a counterpart to this Cu−N vibration band. The weak, low-frequency features at 256 and 297 cm^{-1} are at almost identical frequencies in **2** and **3**, and therefore are likely associated with internal β-diketiminate ligand modes.

Finally, the resonance Raman excitation profile in Figure 5 confirms the ligand $\pi \rightarrow \pi^*$ assignment for the high energy 28500 cm^{-1} (350 nm) electronic transition (band 9) in Figure 2A. Specifically, the Raman spectra of complexes **2**, **3**, (Figure 3B) and the LCuCl starting material (not shown) are very similar using 351 nm (28490 cm^{-1}) excitation energy. Figure 3B demonstrates that the most intense vibrational features in these spectra are at high frequency (545 cm^{-1}, ∼1300 cm^{-1}, and ∼1600 cm^{-1}). These observations confirm that this band is independent of the thiolate (or Cl) ligand (since no enhancement of Cu−S or Cu−Cl stretches is observed). Further, the high frequencies of the strongly enhanced vibrations are consistent with intraligand C−N and/or C−C stretches, which implies that the high intensity of these vibrations derives from considerable distortion along these modes in the excited electronic state at 350 nm. This type of geometric distortion would be expected for an excited electronic state with a π-antibonding interaction between atoms in the β-diketiminate ligand, as would be observed in a π^* state. The fact that resonance Raman profiles reveal that there is some Cu−N excited-state distortion in band 9 is also consistent with it being associated with a ligand π^* excited state. A transition from an orbital with intraligand nonbonding C−C or C−N interactions to one with antibonding interactions could modulate the strength of the Cu−N interaction, leading to its Raman enhancement. These two arguments strongly argue for assignment of the 350 nm band as an intraligand $\pi - \pi^*$ transition.

3.3.3. Enhancement Profile Analysis and Excited-State Distortion. The resonance Raman enhancement profile (RREP) in Figure 5 shows the excitation wavelength dependence of the Raman spectral intensity relative to an internal intensity standard, in this case solvent bands. This excitation energy dependence of the Raman spectrum is due to the that fact that resonance Raman intensity derives from geometric distortions in the excited electronic state.[52] Since different excitation wavelengths involve resonance with different excited electronic states (and therefore different excited geometries), a different set of vibrational bands can be enhanced with different excitation energies. From Figure 5, the ∼425 cm^{-1} band, which has been assigned above based on ^{34}S isotope shifts as the Cu−S(thiolate) stretch, is strongly enhanced through band 3 ($\lambda_{\max} \approx$ 750 nm $\approx$ 13500 cm^{-1}) of **2**. This vibration is expected to be strongly enhanced in the S $\rightarrow$ Cu CT transition (band 3), since this electronic transition formally involves promotion of an electron from a bonding Cu−S pπ orbital to the HOMO where this interaction is antibonding; leading to a large excited-state distortion in the Cu−S bond. For bands 4−6 no resonance enhancement is observed, consistent with their assignment as d $\rightarrow$ d transitions at higher energy than the S p$\pi \rightarrow$ Cu CT band. Bands 7 and 8 show no resonance enhancement and the RREP provides no further insight into their assignment. In contrast, the β-diketiminate intraligand $\pi - \pi^*$ transition (band 9, $\lambda_{\max}$ = 350 nm) shows substantial resonance enhancement, but a different set of vibrational bands is enhanced (vide supra). Finally, the RREP of complex **3** is similar to that of **2** and shown in Figure S2.

Additional analysis[28−33] of the RREP of the S p$\pi \rightarrow$ Cu CT band makes it is possible to obtain a quantitative estimate of the magnitude of the excited-state distortion of the Cu−S bond associated with this charge-transfer transition.[53,54] Specifically the dimensioned distortion along normal mode Q_{n} (ΔQ_{n}, e.g., a Cu−S stretch, with units of Å) is given by

$$\Delta Q_n = \frac{5.805}{\sqrt{\nu_{\mathrm{n}} \mu_{\mathrm{n}}}} \cdot \Delta \qquad (1)$$

where Δ is a dimensionless normal-coordinate displacement parameter, ν_{n} is the modal frequency (in cm^{-1}), and μ_{n} is the

---

[52] Spiro, T. G.; Czernuszewicz, R. S. *Methods Enzymol.* **1995**, *246*, 416−460.

[53] Gamelin, D. R.; Bominaar, E. L.; Mathonière, C.; Kirk, M. L.; Wieghardt, K.; Girerd, J.-J.; Solomon, E. I. *Inorg. Chem.* **1996**, *35*, 4323−4335.

[54] Henson, M. J.; Mukherjee, P.; Root, D. E.; Stack, T. D. P.; Solomon, E. I. *J. Am. Chem. Soc.* **1999**, *121*, 10332−10345.

Table 3. Parameters for Fits of the S pπ → Cu CT Band in **2** (Γ = 500 cm^{-1})

$\nu(i)$/cm^{-1}	$\Delta(i)$	$E_R(i)$/cm^{-1}	% contrib
428	2.08	930	83
540	0.05	1	0
1300	0.05	2	0
370	1.00	185	17
		total E_R 1120	

molecular reduced mass (in g/mol). The absolute magnitude of the dimensionless normal-coordinate displacement parameter, Δ, is determined from a time-dependent[28−33] simulation of the absorption spectrum and the Raman enhancement profile using a self-consistent set of parameters (Figure 5).

The parameters used to simulate successfully the experimental data for **2** are summarized in the first two columns of Table 3. For the S pπ → Cu CT band at 752 nm in **2**, both the 370 and 428 cm^{-1} bands show enhancement with Δ values of 1.0 and 2.1, respectively. In contrast, the π−π* band at 350 nm shows strong enhancement of the 1300, 540, and 370 cm^{-1} vibrations that have absolute Δ values of 1.2, 1.4, and 1.0, respectively. The excited-state vibrational relaxation energy, E_R, corresponds to the total amount of vibrational energy of the individual modes associated with the difference in electronic structure upon changing from the ground state to the excited state, that is, $E_R = \Sigma_i E_R(i) = \Sigma_i\, 1/2\, k_i\, (\Delta Q_i)^2$. The vibrational relaxation energy of the different modes ($E_R(i)$) can also be determined by relating the Δ values determined above to the Huang−Rhys parameter S: $S_i = E_R(i)/\nu_i = \Delta^2_i/2$.[46,53,55] The second relationship gives the relaxation energies for the S pπ → Cu CT band of **2** that are included in Table 3. The total relaxation energy is much smaller for **2** (1100 cm^{-1}) than for **1** (2600 cm^{-1}). As expected, the largest contribution (85%) to this energy is associated with the Cu−S stretching mode (Table 3).

To approximate the vibrational system so that the excited state distortion can be determined, we consider only the Cu−S fragment and that the 428 cm^{-1} mode corresponds to a stretch of this fragment. The strong relative intensity of this band in the rR spectrum in Figure 3 suggests that this is a reasonable approximation. Equation 1 can now be used to determine the excited-state distortion. Within this approximation, the dimensioned distortion along the normal coordinate (ΔQ) directly relates to the change in the Cu−S distance (i.e., $\Delta r = \Delta Q$). Since in the excited state, an electron occupies the S pπ antibonding orbital at the expense of the bonding orbital, the distortion will, in fact, be an elongation along this bond. Based on this analysis, the Cu−S elongation in the S pπ → Cu CT excited state of **2** is 0.12 Å, which is significantly smaller than that for complex **1** (0.20 Å).[20] This is largely due to the smaller magnitude of the dimensionless normal-coordinate displacement parameter, Δ, value for **2** (Δ = 2.1) relative to **1** (Δ = 3.3). Since both complexes incorporate the same sterically hindered triphenylmethylthiolate, the differences between the CT excited-state distortions are due to the effects of differences in the Cu−N interactions on the thiolate−Cu bond (vide infra).

3.4. Metal and Ligand XAS Spectroscopy. XAS experiments at the S K- and Cu L-edges can provide quantitative information about the electronic structure of a complex including details of the HOMO wave function character.[56,57] Specifically, the S and Cu characters in the HOMO ($\Psi_{HOMO} \approx [1 - \alpha^2]^{1/2} |\text{Cu 3d}\rangle - \alpha\, |\text{S 3p}\rangle$) can be directly probed by measuring the intensities of the dipole allowed S 1s → HOMO or Cu 2p → HOMO transitions, while the relative energies of the edge and preedge features in the spectra give further insight into the electronic structure.

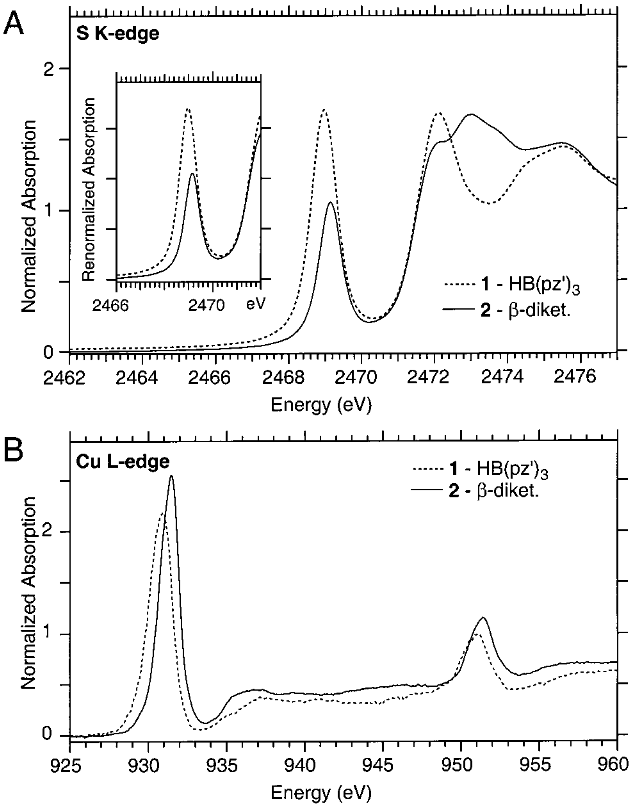

Figure 6. XAS spectra of complexes **1** and **2**. (A) S K-edge spectra. (B) Cu L-edge spectra. Complex **1** − dotted line; Complex **2** − solid line. Table 4 presents key spectral metrics.

Table 4. S K-edge and Cu L-edge XAS Data

S K-edge data: compound	preedge energy (eV)[a]	preedge intensity[b]	%S covalency[b]
1	2469.0	1.28	52 ± 1.2
2	2469.2	0.85	32 ± 2.5

Cu L-edge data: compound	peak positions (eV)[a]		peak intensities		%Cu covalency[b]
	L_2	L_3	L_2	L_3	
1	930.8	950.8	4.07	1.04	36 ± 0.4
2	931.3	951.3	3.68	0.97	33 ± 0.8

[a] Energies reported are within an error of ±0.1 eV. [b] Error reported is the standard deviation of all good fits, an additional 3−4% error is introduced by the normalization procedure.

3.4.1. Intensities. The S K-edge spectrum of complex **2** is compared to that of complex **1** in Figure 6A. Using plastocyanin as a reference with 38% S 3p character in the HOMO,[58] the intensity of the preedge feature in the S K-edge XAS spectrum of **2** gives 32% S 3p character in the HOMO (Table 4). In contrast, the HOMO of complex **1** shows 52% S p character.[20] Thus, in **2** there is substantially less S p character in its HOMO, even though this complex utilizes the same triphenylmethylthiolate ligand as **1**. This difference in thiolate S character in the HOMO reflects the effect of the difference in the nitrogen ligation for the two systems. Finally, the reduced S 3p character

---

(55) Huang, K.; Rhys, A. *Proc. R. Soc., London A* **1951**, *208*, 352.

(56) Hedman, B.; Hodgson, K. O.; Solomon, E. I. *J. Am. Chem. Soc.* **1990**, *112*, 1643−1645.

(57) Glaser, T.; Hedman, B.; Hodgson, K. O.; Solomon, E. I. *Acc. Chem. Res.* **2000**. In press.

(58) Shadle, S. E.; Penner-Hahn, J. E.; Schugar, H. J.; Hedman, B.; Hodgson, K. O.; Solomon, E. I. *J. Am. Chem. Soc.* **1993**, *115*, 767−776.

in the HOMO of **2** relative to **1** is consistent with the substantially reduced oscillator strength in the absorption spectrum noted previously.

The Cu L-edge XAS spectra of complexes **1** and **2** are compared in Figure 6B. Using D_{4h} $[\mathrm{CuCl_4}]^{2-}$ as a reference complex with 61% Cu character in its HOMO,[59] the HOMO of **2** has 33% Cu character (Table 4). This is slightly less than the 36% Cu character observed for **1**. Although the combined S and Cu covalencies determined with this XAS analysis imply a covalent thiolate interaction in **2**, they account for only ~65% of the total wave function character. This suggests that there is another significant covalent interaction in the HOMO of **2**. The large ^{14}N superhyperfine coupling observed in its EPR spectrum[19] implies that this covalency is contributed by N character in the HOMO of **2** (vide infra). In addition, Cl K- and Cu L-edge XAS of the chloride analogues of **1** and **2** indicates similar Cl covalency in both complexes, but increased Cu character in the Cl analogue of **1** (73% Cu character) relative to the Cl analogue of **2** (48% Cu character) (see Supporting Information, Figure S3), further supporting the significant contribution from the β-diketiminate ligand in the ground-state wave function of **2**.

3.4.2. Edge and Preedge Energies. The energies of the S K-edge feature $|\mathrm{S}\ 1s\rangle \rightarrow |\mathrm{S}\ 4p\rangle$ for **1** and **2** both exhibit a first derivative inflection point at 2471.5 eV. This indicates that the sulfur 1s core orbitals lie at similar energies in these two complexes and therefore that the effective nuclear charges of the thiolate sulfurs in these two compounds are virtually identical. This implies that the S(thiolate) atoms in both complexes are similar donor ligands, which is consistent with the similarities of the Raman Cu−S stretching frequencies observed for the two complexes. The sulfur preedge feature in **2** occurs at 2469.2 eV (Table 4) and is 0.2 eV higher than the preedge feature in complex **1**. Because the edge energies of these two compounds are so close, the preedge energy difference represents the combined effects of shifts in the entire d-orbital manifold due to changes in the Z_{eff} of Cu and differences in the ligand field splitting (vide infra).

The Cu L-edge XAS spectra presented in Figure 6B show that both the L_3 (~931 eV) and L_2 (~951 eV) edges are about 0.5 eV higher in **2** than in **1** (Table 4). The energies of the Cu L-edge transitions (Cu 2p → 3d, HOMO) depend on the metal ligand field, the overall energy of the d manifold, and shifts in the Cu 2p core energy level (vide infra).[60]

3.4.3. XAS Comparison of 1 to 2. Contained in XAS preedge energies is information about the relative effective nuclear charge (Z_{eff}) of the copper atom in complexes **1** and **2**. However, the preedge energy has contributions from the ligand field splitting, the energy of the entire d-manifold, which is affected by Z_{eff}, and the core level energies. A more positive Z_{eff} for Cu will shift the entire d-manifold to deeper binding energy.[60] By examining the relative preedge and edge energies in **1** versus **2** at the Cu L- and S K-edge regions, we can determine the relative Z_{eff} values for the two complexes. Scheme 1 summarizes the three possibilities for the relative Z_{eff} of Cu in the two complexes: (i) if Z_{eff} in **1** were equal to Z_{eff} in **2**, their d-manifolds would be at identical energies; (ii) if Z_{eff} in **1** were more positive than in **2**, the d-manifold of the latter would be to less deep binding energy; (iii) if Z_{eff} in **1** were less positive than in **2**, the d-manifold of the latter would be at deeper binding energy. Based on the similar edge energies in the S K-edge data for the two complexes, the S(thiolate) 1s core levels are at the same energy in **1** and **2**. Further, the MCD results (Figure 2B) make it clear that the ligand field of **2** is larger than in **1**, with the average energy of the "initial state" d → d transitions in **2** being 6800 cm^{-1} (~0.8 eV) higher than in **1**.[20] Including this information for these three cases, the pattern of S K− and Cu−L preedge transition energy shifts for complex **2** relative to **1**, $\Delta_{\mathrm{S-K}}^{\mathbf{2-1}}$ and $\Delta_{\mathrm{Cu-L}}^{\mathbf{2-1}}$, in Scheme 1 can be predicted. Application of this analysis to the observed XAS data will enable us to evaluate the Z_{eff} of Cu in **2** relative to that in **1**.

Scheme 1

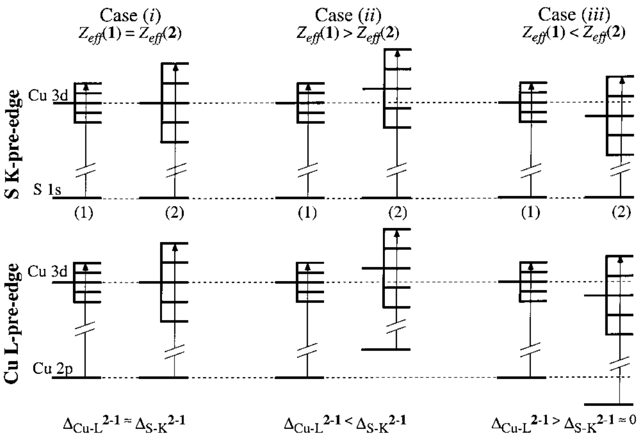

If the Z_{eff} of Cu in **1** and **2** were equal, case (i), ligand field effects alone, which are observed with optical spectroscopy (vide supra), would dominate the shifts of the preedge features in XAS spectra. This suggests that both the S K− and Cu−L-preedges for **2** should be at higher energy than for **1** by a similar amount that would correspond to the "final state" ($|d^{10}\underline{c}\rangle$)[61] ligand field difference of the two complexes (i.e., $\Delta_{\mathrm{Cu-L}}^{\mathbf{2-1}} \approx \Delta_{\mathrm{S-K}}^{\mathbf{2-1}}$). The magnitude of the experimentally observed shifts in the S K- and Cu L-preedge features are not equivalent (0.2 eV for S K-edge and 0.5 eV for Cu L-edge); thus, this case does not apply. In case (ii), the decreased Z_{eff} of **2** relative to **1** would shift both the core Cu 2p orbitals and the valence orbitals to less deep binding energy, but the magnitude of the effect on the core orbitals should be greater. This suggests that the Cu L-edge transition of **1** would be at higher energy than for **2**. Further, the decreased Z_{eff} of **2** relative to **1** would combine with the larger ligand field of **2** to give a large S K-preedge transition energy difference. In addition to the incorrect prediction of the relative Cu L-preedge energies of **2** and **1**, the predicted S K-preedge and Cu L-preedge differences ($\Delta_{\mathrm{Cu-L}}^{\mathbf{2-1}}$ and $\Delta_{\mathrm{S-K}}^{\mathbf{2-1}}$) for this case are reversed from what is observed experimentally. It is therefore clear that Z_{eff} of **1** is not greater than or equal to Z_{eff} of **2**. Finally, in case (iii), for the S K-preedge energy, the increased ligand field of **2** would be offset by its higher Z_{eff} relative to that of **1**. These two effects would largely cancel, leading to a small S K-preedge energy difference between **1** and **2**. At the Cu L-edge, the increased relative Z_{eff} of **2** would shift both the core and valence orbitals to deeper binding energy, though again the magnitude of the shift in the core Cu 2p orbitals would be expected to be larger. Therefore the Cu L-preedge transition energy of **2** would be expected to be at higher energy than the transition of **1**. Only case (iii) predicts an energy shift pattern for both the Cu L-edge and S K-edge data that is consistent with experiment. This clearly demonstrates that the Z_{eff} of the copper atom in **1** is less positive than that of the Cu in **2** and further implies that the d-manifold

---

[59] George, S. J.; Lowery, M. D.; Solomon, E. I.; Cramer, S. P. *J. Am. Chem. Soc.* **1993**, *115*, 2968−2969.

[60] Shadle, S. E.; Hedman, B.; Hodgson, K. O.; Solomon, E. I. *Inorg. Chem.* **1994**, *33*, 4235−4244.

[61] This represents the metal valence configuration after formation of core hole denoted by $\underline{c}$.

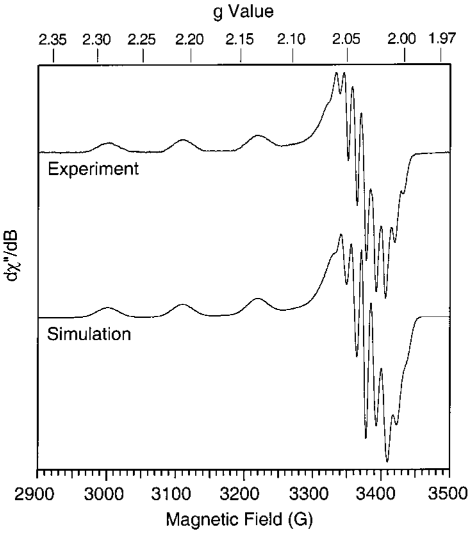

Figure 7. EPR spectrum of **2** and a simulation with the nitrogen superhyperfine interactions aligned with their z' directions along the Cu−N bonds. Parameters are summarized in the text. Experimental spectrum from ref 19.

of complex **2** lies to deeper energy than in complex **1**. In summary, this analysis of the relative XAS preedge energies indicates that the effective nuclear charge on the Cu is higher in the three [2N + S] coordinate **2** than in the four [3N + S] coordinate **1**. These results clearly indicate that, while the β-diketiminate is a strong in-plane donor ligand that leads to reduced S pπ character in the HOMO, the additional ligand in the axial position of the tris(pyrazolyl)hydroborate ligand provides a stronger net donor interaction with the Cu.

3.5. Analysis of Nitrogen Superhyperfine Coupling in the EPR Spectrum. The EPR spectrum of **2** reveals a strong nitrogen superhyperfine interaction in the $g_\perp$ region,[19] as shown in Figure 7. In contrast, no ^{14}N superhyperfine coupling is resolved in the EPR spectra of either fungal laccase or **1**.[15,23,62,63] This suggests that there is considerable nitrogen character in the HOMO of **2**. For the ligating N atoms to exhibit considerable covalency, the HOMO must be oriented in the trigonal N_2S plane. Using simulations of the EPR spectrum that include this superhyperfine interaction, the degree of N covalency can be quantitated. To obtain this molecular information, it is necessary to simulate the EPR spectrum with the ^{14}N hyperfine interaction matrix (‘tensor’) aligned with its z direction (z') along the Cu−N bond. This axis system is different than the molecular axis system employed in the earlier EPR simulations where z is perpendicular to the HOMO plane. Thus, the superhyperfine interaction matrix must be rotated into this molecular axis system in the spectral simulations. The spin Hamiltonian parameters used in the slightly revised EPR simulation shown in Figure 7 are: $g_x = 2.037$, $g_y = 2.037$, $g_z = 2.169$, $A_x(\mathrm{Cu}) = 4.7 \times 10^{-4}$ cm^{-1} (14 MHz), $A_y(\mathrm{Cu}) = 9.3 \times 10^{-4}$ cm^{-1} (28 MHz), $A_z(\mathrm{Cu}) = 106.7 \times 10^{-4}$ cm^{-1} (320 MHz), $A_x'(\mathrm{N}) = 10 \times 10^{-4}$ cm^{-1} (30 MHz), $A_y'(\mathrm{N}) = 10 \times 10^{-4}$ cm^{-1} (30 MHz), $A_z'(\mathrm{N}) = 14 \times 10^{-4}$ cm^{-1} (42 MHz), where the two $I = 1$ ^{14}N atoms differ only in their Euler angles and the prime on the nitrogen HF parameters indicate that the directions are in the ligand axis system (i.e., Cu−N direction = z'); here the molecular (g and Cu hyperfine) axis system places z perpendicular to the N_2S plane.[64]

The isotropic portion of the observed nitrogen superhyperfine interaction results from Fermi contact with the N 2s character that is mixed into the σ-bonding ligand MO by hybridization, while the anisotropic portion results from spin dipolar coupling between the ^{14}N nuclear spin and the unpaired (anisotropically distributed) electron character in the N pz orbital that lies along the Cu−N bond.[65,66] The noncovalent electron−nuclear dipolar coupling is a small fraction (5%) of these parameters; it is not included in this analysis because it is on the order of the uncertainty of the simulated values. Ligand field theory expressions for the superhyperfine parameters $A_\|(^{14}\mathrm{N})$ and $A_\perp(^{14}\mathrm{N})$ can be written as:[65]

$$A_\|(^{14}\mathrm{N}) = \beta^2\left(\frac{1}{2}\right)\cdot\{n^2 A_{\mathrm{Iso}}^{^{14}\mathrm{N}} + (1-n^2)A_{\mathrm{Aniso}}^{^{14}\mathrm{N}}\} \tag{2a}$$

$$A_\perp(^{14}\mathrm{N}) = \beta^2\left(\frac{1}{2}\right)\cdot\{n^2 A_{\mathrm{Iso}}^{^{14}\mathrm{N}} - {}^1/_2(1-n^2)A_{\mathrm{Aniso}}^{^{14}\mathrm{N}}\} \tag{2b}$$

Here β^2 is the total nitrogen covalency (i.e., HOMO nitrogen wave function character) and n^2 represents the degree of s hybridization of the β-diketiminate ligand orbital (i.e., $\Psi_{\mathrm{N,b1}} \approx \sqrt{[1-n^2]}\ |\mathrm{N\ 2pz}\rangle + n|\mathrm{N\ 2s}\rangle$). The quantities $A_{\mathrm{iso}}^{^{14}\mathrm{N}}$ and $A_{\mathrm{Aniso}}^{^{14}\mathrm{N}}$ are calculated isotropic and anisotropic hyperfine couplings of one unpaired electron residing in the respective nitrogen orbitals (2s and 2pz) and are tabulated[65,67] ($A_{\mathrm{iso}}^{^{14}\mathrm{N}} \approx 520 \times 10^{-4}$ cm^{-1} and $A_{\mathrm{Aniso}}^{^{14}\mathrm{N}} \approx 31 \times 10^{-4}$ cm^{-1}). The factor of $^1/_2$ outside of the braces corrects for the two symmetry-related nitrogens in the HOMO. The parameters β^2 and n^2 in eqs 2 are both unknown. However, solving eqs 2 simultaneously using the experimentally determined superhyperfine values of $A_\|'$ and $A_\perp'$ gives $\beta^2 = 0.2-0.3$ and $n^2 = 0.1-0.2$. In addition to showing moderate s hybridization, this analysis demonstrates that the HOMO of **2** has significant (~25% N) nitrogen covalency. This substantial N covalency accounts for the majority of the HOMO wave function character that was outstanding from the S K-edge and Cu L-edge XAS experiments (vide supra). The small remaining wave function character (~10%) apparently resides on nonligating atoms including those in the β-diketiminate ligand as well as the triphenylmethyl group.

The magnitude of the nitrogen superhyperfine and the degree of covalency that it indicates attest to considerably larger ground-state nitrogen covalency for **2** than for either complex **1** or for blue Cu centers such as fungal laccase or plastocyanin, where no nitrogen superhyperfine is observed in the EPR spectrum. Higher resolution EPR-derived spectroscopic techniques have not been applied to **1**, and it is not possible to make a quantitative comparison between the model complexes. However, based on ENDOR studies of several blue Cu sites, Hoffman et al. have estimated a much lower N-ligand covalency of ~5% N per ligand.[68] The large N covalency in the HOMO of **2** is consistent with its reduced S p covalency observed with XAS (vide supra).

---

[62] Kitajima, N. *Adv. Inorg. Chem.* **1992**, *39*, 1−77.

[63] Penfield, K. W.; Gay, R. R.; Himmelwright, R. S.; Eickman, N. C.; Norris, V. A.; Freeman, H. C.; Solomon, E. I. *J. Am. Chem. Soc.* **1981**, *103*, 4382−4388.

[64] The EPR parameters in the text were simulated using first-order perturbation theory. (Neese, F.; Zumft, W. G.; Antholine, W. E.; Kroneck, P. M. H. *J. Am. Chem. Soc.* **1996**, *118*, 8692−8699.) Matrix diagonalization approaches with QPOWA[26] gives a slightly (~4%) larger value for A_z(Cu) of 111 × 10^{-4} cm^{-1} (332 MHz).

[65] Goodman, B. A.; Raynor, J. B. *Adv. Inorg. Chem. Radiochem.* **1970**, *13*, 135−362.

[66] McGarvey, B. R. In *ESR and NMR of Paramagnetic Species in Biological and Related Systems*; Bertini, I., Drago, R. S., Eds.; D. Reidel: Dordrecht, Holland, 1980; pp 171−200.

[67] Herman, F.; Skillman, S. *Atomic Structure Calculations*; Prentice Hall: Englewood Cliffs, NJ, 1963.

[68] Werst, M. M.; Davoust, C. E.; Hoffman, B. M. *J. Am. Chem. Soc.* **1991**, *113*, 1533−1538.

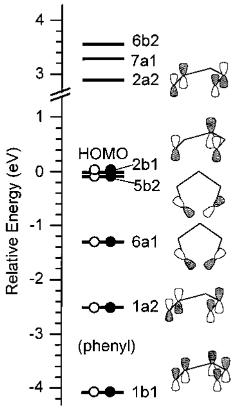

Figure 8. Calculated energy level diagram and orbital representations for the high-lying valence orbitals of the β-diketiminate ligand. Key orbitals are described in the text.

3.6. Density Functional Calculations. The experimentally derived spectral features that have been described above for **2** relative to **1** include the following: the d → d transitions are at higher energy; the S pπ → Cu CT transition is at lower energy and of lower intensity; the Cu−S bonds exhibit similar strength; the excited-state distortion, Δ_{ES}, is significantly reduced; the HOMO has similar Cu character, reduced S(thiolate) character, and enhanced N character; and the Cu Z_{eff} value is more positive. These data can now be used to evaluate electronic structure calculations which can give further insight into bonding. First, the β-diketiminate ligand system is defined. Subsequently, the electronic structure of the Cu(II)-thiolate complex of this ligand **2** is evaluated and compared to complex **1**.

3.6.1. Valence Orbitals of the Ligands.

3.6.1.1. β-Diketiminate Valence Orbitals. The electronic structure of the planar, conjugated β-diketiminate ligand core, which is modeled as $C_3N_2H_5$, is an important aspect of the electronic structure of Cu complex **2** and permits an evaluation of the equatorial ligand interaction. Note that the phenyl rings that are appended to the nitrogens of this ligand are perpendicular to the C_3N_2Cu plane[19] and are not part of the conjugated π-system. Figure 8 shows an energy level diagram determined by ADF calculations with schematic representations of the highest energy β-diketiminate orbitals that might be involved in bonding interactions with Cu. In this anionic ligand, the two highest-lying orbitals are close in energy ($\Delta E < 0.2$ eV). The HOMO (2b1) is characterized by out-of-plane p-type orbitals on the two nitrogens and the central carbon (C3). In contrast, the 5b2 orbital is characterized by in-plane, out-of-phase orbitals localized on the nitrogens with lobes that point directly toward the metal (Figure 8). In 5b2, the wave function character is calculated to be mostly (39% N_{calc} per N) in the hybridized N orbitals which would interact with the coordinated Cu. In contrast, in the 2b1 orbital the wave function character is distributed among the out-of-plane orbitals on C3 (37% C_{calc}) and the terminal Ns (28% N_{calc} per N). To deeper energy lies the 6a1 orbital, an in-plane, in-phase analogue of 5b2 that could also take part in ligand−metal bonding, though it would be expected to be weaker since the energy denominator would be larger. To still deeper binding energy lie the out-of-plane 1a2 and 1b1 orbitals that are unlikely to have significant interactions with the metal orbitals. Between these last two orbitals lie the highest phenyl ring derived orbitals (not shown). The LUMO of the β-diketiminate ligand (2a2) is also important in the spectroscopy of the complex (e.g., the ligand $\pi \rightarrow \pi^*$ transition at 350 nm, vide supra). The LUMO is characterized as the π-antibonding analogy of 1a2. The HOMO−LUMO gap of the ligand used (including the phenyl ligands) is 2.3 eV.

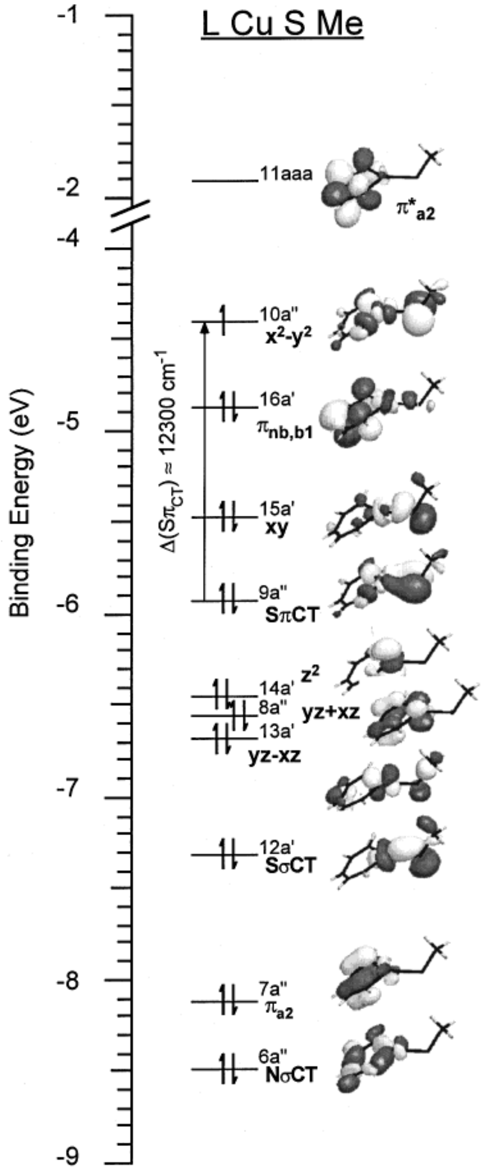

Figure 9. Calculated energy level diagram and orbital representations for the occupied, high-lying valence orbitals of complex **2** (β-diketiminate trimethylthiolate Cu(II)). The β-diketiminate-localized LUMO is also included. See Table 5 for a summary of the calculated wave function characters.

3.6.1.2. Thiolate. The thiolate orbitals were discussed fully in the preceding paper.[20] Briefly, the two important valence orbitals that can interact strongly with the Cu d orbitals are designated S pπ and S p pseudo-σ. These are the p orbitals on the sulfur that do not interact with the alkyl carbon. The Cu−S−C angle splits the energy of these orbitals. Further, the Spπ orbital can undergo a π-symmetry interaction with the $d_{x^2-y^2}$ orbital, while the S p pseudo-σ orbital is oriented perpendicular to the C−S bond and the S pπ orbital.

3.6.2. Description of Bonding in 2 and Comparison to Spectra. An energy diagram of complex **2**, as calculated with DFT including the generalized gradient approximation as implemented in the ADF package,[38,39] is shown in Figure 9 along with representations of the highest lying molecular orbitals. The wave functions of these orbitals are summarized in Table 5. Three key orbitals, the HOMO (10a″), the Cu−S

Table 5. Results of ADF Calculations for the Highest Valence Orbitals in the [$C_3H_5N_2$ $CuSCH_3$] Approximation to **2**

	molecular orbital labels										
	10 A″ x^2-y^2	16A′ $\pi_{nb,b1}$	15A′ d_{xy}	9A″ S pπ	14A′ d_{z^2}	8A″ d_{yz+xz}	13A′ d_{yz-xz}	12A′ S ps. σ	7A″ op π_{a2}	6A″ Nσ	11A″ LUMO
energy (eV):	−4.403	−4.875	−5.483	−5.933	−6.459	−6.563	−6.695	−7.311	−8.123	−8.491	−1.907
orb. contrib.											
Cu d_{z^2}	0	0.2	3	0	17	0	5	6	0	0	0
Cu d_{yz}	0.1	2	2	3	0.7	38	33	12	8	1.6	0.6
Cu d_{xz}	0.1	2	2	3	0.7	38	33	12	8	1.6	0.6
Cu d_{xy}	0	6	10	0	67	0	3	40	0	0	0
Cu $d_{x^2-y^2}$	32	0	0	11	0	1	0	0	5	37	0.0
Cu d total	**32**	**10**	**17**	**17**	**85**	**77**	**74**	**70**	**21**	**40**	**1.2**
Cu s+p total	1	3	9	6	5	0.1	0.7	0.5	0.1	0.1	0.2
S Total	**40**	**5**	**54**	**46**	**0.2**	**1.5**	**7**	**22**	**0.5**	**0.8**	**0.2**
CH_3 Total	2	1	4	4	0.4	0.1	5	4	0.2	0.5	0.0
N Total	**18**[b]	**40**	**7**	**20**	**7**	**8**	**0.9**	**1.6**	**49**	**19**	**34**
β-diket. Lig.[a]	5	36	6	6	1.7	12	10	1.7	28	37	60

[a] Wave function character of the nonliganding atoms in the β-diketiminate ligand. [b] In the HOMO there is 3.13% N 2s character and 15.23% N 2p character.

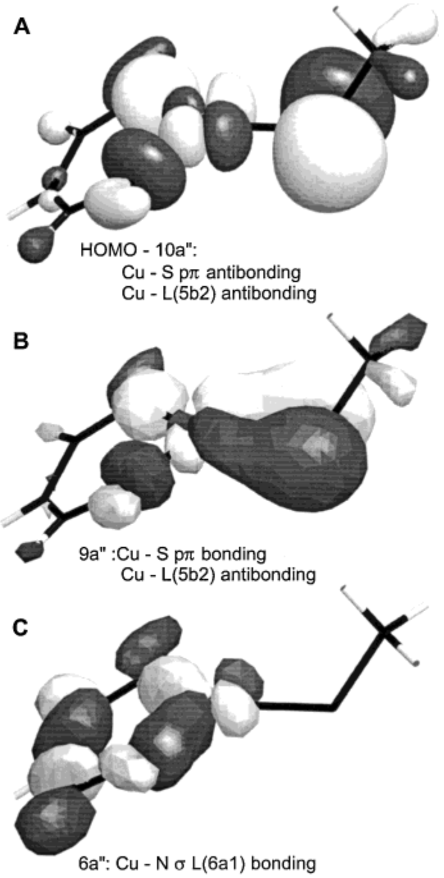

Figure 10. Orbital contours for three important molecular orbitals of complex **2**: (A) Cu $d_{x^2-y^2}$ HOMO (10a″) showing the S pπ antibonding and N σ antibonding interactions; (B) S pπ bonding orbital (9a″) showing its N σ antibonding interaction; and (C) N−Cu bonding orbital (6a″).

pπ bonding orbital (9a″), and the Cu−Nσ bonding orbital (6a″), are detailed in the contours in Figure 10.

3.6.2.1. HOMO. The redox-active, half-occupied HOMO shows the now familiar[11,21,22,69−71] π-type antibonding interaction between the $d_{x^2-y^2}$ and S pπ orbital (Figure 10A). This is similar to the interaction present in the HOMO of **1** and many blue Cu proteins. In analogy to **1** and blue Cu proteins, where this interaction was first observed,[21,69] the calculations indicate that this interaction is very covalent with 32% Cu d_{calc} and 40% S_{calc} (Table 5). The Cu $d_{x^2-y^2}$ character calculated for the HOMO is supported by the positive shift in the EPR g-values from g_e (=2.0023), i.e., $g_{||} > g_\perp > g_e$. The calculations faithfully reproduce the relatively small Cu character (32% Cu d_{calc}) obtained from the Cu L-edge measurements (33% Cu d). Further, the significant thiolate covalency in the calculations is consistent with the S covalency of the HOMO of **2** that was measured with S K-edge XAS. Importantly, the calculations reproduce the decreased thiolate character of **2** (40% S_{calc}) relative to **1** (49% S_{calc}), though not to the extent observed experimentally with S K-edge XAS (32% S for **2** vs 52% S for **1**). The reduction in the calculated thiolate character in the HOMO of **2** is consistent with its reduced oscillator strength relative to **1**. Also, consistent with experimental observation, the calculations reproduce the shift in HOMO wave function character from the thiolate ligand to the N-ligand in **2** versus **1**, while the Cu character remains approximately constant. The HOMO is also calculated to exhibit considerable (18% N_{calc}) nitrogen character which derives from an antibonding interaction between the Cu orbitals and the 5b2 orbital of the β-diketiminate ligand. The large N character calculated in the HOMO (18% N_{calc}) agrees reasonably well with the experimental covalency ($\beta^2_{expt} = 0.2-0.3$) and s−p hybridization ($n^2_{expt} = 0.1-0.2$) derived above from the significant ^{14}N hyperfine observed in the EPR spectrum.[19,72] Thus, the calculations quite reasonably reproduce many key experimentally derived ground-state properties of **2**, and reproduce ground state differences between **1** and **2**.

3.6.2.2. Excited Electronic States. Spectral Patterns and Assignments for 2. The calculated one-electron energies reflect the experimental trends in the relative energies of the excited states. To 0.5 eV deeper binding energy than the HOMO in Figure 9 lies the nonbonding 2b1 β-diketiminate-based MO ($\pi_{nb,b1}$ or 16a′). Next, the calculations predict that the d_{xy} orbital (15a′) has an antibonding interaction with the S p pseudo-σ orbital. In the middle of the ligand field levels lies the S pπ bonding orbital (9a″). Due to significant ligand orbital-ligand orbital overlap between MO 9a″ (S pπ-Cu bonding, Figure 10B) and the HOMO of **2** (Figure 10A) which relates to the absorption

---

(69) Penfield, K. W.; Gewirth, A. A.; Solomon, E. I. *J. Am. Chem. Soc.* **1985**, *107*, 4519−4529.

(70) Larsson, S.; Broo, A.; Sjölin, L. *J. Phys. Chem.* **1995**, *99*, 4860−4865.

(71) Pierloot, K.; Dekerpel, J. O. A.; Ryde, U.; Roos, B. O. *J. Am. Chem. Soc.* **1997**, *119*, 218−226.

(72) Using the values of β^2 and n^2 calculated with DFT (Table 5), the ^{14}N superhyperfine parameters can be calculated to be $A_{||,\,calc}' \approx 12 \times 10^{-4}$ cm^{-1} and $A_{\perp,\,calc}' \approx 8 \times 10^{-4}$ cm^{-1} in good agreement with the experimental values of 14×10^{-4} cm^{-1} and 10×10^{-4} cm^{-1}.

intensity, it is clear that a transition from the 9a″ orbital to the HOMO (10a″) yields the intense, low-energy S pπ CT transition. Clustered, to deeper binding energy than the S pπ bonding orbital are the d_{z^2}, d_{yz-xz}, and d_{yz+xz} orbitals. Below these orbitals lie the S p pseudo-σ bonding orbital, the β-diketiminate-derived 1a2 orbital, which has a weak δ-type bonding interaction with the Cu d_{yz+xz} orbital, and the N σ-bonding orbital. The spectral pattern predicted by the calculations in which the S pπ → Cu CT band is embedded in the LF bands is consistent with experiment (Figure 2). However, the calculations reverse the observed order of the d_{z^2} and d_{xy} orbitals. The assignment from experiment (in Table 1) is consistent with the EPR-derived $g_{||}$ value, which provides an independent measure of the relative d_{xy} → HOMO transition energy.[73] Only assigning the higher energy of these two d → d bands as d_{xy} gives the correct correlation between MCD and EPR spectral results over a series of blue Cu proteins.[15]

Further, the calculations provide insight into the unassigned bands 2, 7, and 8 observed in the absorption and MCD spectra (Figure 2). Band 2 is likely due to a $\pi_{nb,b1}$ → HOMO transition, which is calculated at fairly low energy. However, the relative ordering of $\pi_{nb,b1}$ and the lowest-energy LF transition is reversed in the calculations. Candidates for bands 7 and 8 in Figure 2 are two of the three deep-lying orbitals in Figure 9: S p pseudo-σ, β-diketiminate π_{a2}, and Nσ. Since the HOMO exhibits considerable N covalency the Nσ→HOMO absorption would be expected to exhibit an intense absorption, which is not the case for band 7 or 8. Further, Raman excitation into the Nσ → HOMO CT transition should give substantial excited-state distortion and therefore a large Raman enhancement. Figure 5 demonstrates that these bands show very little Raman enhancement at any vibrational frequency, further arguing against their assignment as Nσ. Based on their calculated energy positions and similarities in MCD sign with analogous copper thiolate systems where the pseudo-σ band is positive, we suggest that band 7 is the S p pseudo-σ → HOMO transition and band 8 involves a β-diketiminate π_{a2} orbital whose MCD intensity derives from the weak δ-type interaction. The Nσ → HOMO transition likely lies among the bands to higher energy than 9. Finally, the calculated LUMO for the complex is localized on the β-diketiminate ligand and analogous to the out-of-plane π* 2a2 orbital in the free ligand (Figures 8 and 9). The high frequency of the Raman vibrations (Figure 3B) that are resonance enhanced in band 9 suggests that this band is associated with a large excited-state distortion along C−C or C−N bonds. Such a distortion would be expected for an electronic transition from $\pi_{nb,b1}$ to π_{a2}*, where the C−N π interactions in the β-diketiminate ligand go from nonbonding to antibonding, which supports the assignment for this band.

3.6.2.3. Excited-State Comparison to 1. These calculations also reproduce the observed spectroscopic trends in compound **2** relative to compound **1**. Specifically, in **2** the S pπ − Cu bonding orbital is calculated to be embedded in the d orbital block (Figure 9), while the calculations on **1** placed the thiolate S pπ bonding orbital to deeper binding energy than the ligand field block, consistent with experimental observation (Figure 2). In addition to the relative position of the CT transition, the calculations also predict the experimental red-shift of the CT transition: in **2** the difference between the one-electron orbital energies of the HOMO and the S pπ bonding orbital is ~2000 cm^{-1} less than the analogous difference in **1**. The calculations also reproduce the substantial blue-shift of the ligand field transitions in **2** relative to **1**. A metric of this in **1** versus **2** is the difference between the one-electron energies of the deepest d orbital (d_{yz-xz}) and the HOMO ($d_{x^2-y^2}$), (Δd−d$_{max}$). By this measure, the calculated LF splitting in **2** is 10500 cm^{-1} larger than in **1**, in reasonable agreement with the experimental difference of 8700 cm^{-1}. Thus, the calculations reproduce the decrease in the energy of the S pπ → Cu CT transition and the higher energy of the d → d bands observed in the MCD spectrum effected by the stronger, trigonal ligand field in complex **2** compared to complex **1**.

Table 6. Comparison of Total Cu 4s + 4p Contributions to Cu−S π and σ Bonding and Antibonding Orbitals

Cu orbital	HB(pz′)$_3$ **1**[a]	β-ket. **2**[a]
4s	1.84	5.47
4pz	0.72	0.37
4p σ	4.16	3.79
4p π	3.52	6.44
total p	8.40	10.60
total s + p	10.24	16.07

[a] The values are percent of an electron

3.6.3. Insights from the Calculations. The above points clearly demonstrate that the ADF density functional electronic structure calculations reproduce experimental trends reasonably well. Therefore, we are now in a position to use the calculations to gain further insight into the differences in the electronic structures of **2** and **1**.

3.6.3.1. Strength of the Thiolate Bond. The calculations reflect the decrease in S thiolate p character in the HOMO of **2** relative to **1** that was observed with the S K-edge experiments. This results from strong interaction in the HOMO and the Cu S pπ bonding orbital between the Cu $d_{x^2-y^2}$ and the β-diketiminate ligand orbital concomitant with a weaker thiolate S pπ − Cu $d_{x^2-y^2}$ interaction as seen in Figures 10A and 10B. Thus, in **2** there appears to be a *trans* influence in which the greater donor strength of the β-diketiminate ligand reduces the strength of the thiolate S pπ interaction with the Cu $d_{x^2-y^2}$ orbital.

The reduced S pπ character in the HOMO derived from experimental and computational results might appear to be inconsistent with Raman data that suggests the total strength of Cu−S bonds are similar in complexes **1** and **2**, because the thiolate S−Cu vibrational frequency is so similar for the two complexes (421 cm^{-1} in **1** versus 428 cm^{-1} in **2**). However, the calculations (Table 6) indicate that there is more 4s and 4p character in the S pπ and S pσ bonding and antibonding orbitals of **2** (10a″ = $d_{x^2-y^2}$, 15a′ = d_{xy}, 9a″ = S pπ, and 12a′ = S pseudo-σ) relative to the analogous orbitals in **1**. The Cu 4pπ (orbital lobes in the equatorial plane but perpendicular to the Cu−S bond) and 4s interactions in **2**, in particular, are significantly larger than in **1**. These MOs reflect enhanced S bonding interactions in **2** with these Cu orbitals relative to **1**, which compensates for the reduced S pπ-type interaction. Thus, while the S pπ character in the HOMO is different between the two complexes, their net Cu−S bonding interactions are very similar. The calculations suggest that this is due to thiolate-Cu orbital interactions that were not reflected in the sulfur K-edge intensity.

3.6.3.2 Behavior of the Low-Energy S pπ CT Transition. On the basis of the experimental evidence presented above it is clear that the 750 nm band in **2** is the S pπ → Cu CT transition. The calculations support this assignment. While the oscillator strength of this band is reduced relative to **1** ($f_{exp,sc}$(**2**) = 0.066 vs $f_{exp,sc}$(**1**) = 0.077, vide supra), in complex **2** this band still exhibits significant intensity, reflecting a covalent Cu−S pπ

---

(73) Since the shift in the $g_{||}$ value from g_e ($\Delta g_{||} = g_{||} - g_e$) is inversely proportional to the d_{xy}→HOMO transition energy, assigning the lower energy d→d band (band 1) as d_{xy} would predict a much greater $\Delta g_{||}$ than is experimentally observed, see ref 15.

bonding interaction. In fact, the quantitative intensity ($f_{\mathrm{exp,sc}}$) of the S pπ → Cu CT band in **2** (band 3) is higher than might be expected considering the S K-edge XAS experiments that indicate the S p character in the HOMO of **2** (32% S p) is substantially reduced relative to **1** (52% S p). An additional contribution to f_{exp} in **2** not present in **1** is the β-diketiminate ligand, which can also contribute to the intensity of this transition. Figure 10, A and B, shows that in **2** there are strong σ-type Cu−N antibonding interactions in both the S pπ − Cu antibonding orbital (HOMO) (18% N_{calc}) and S pπ bonding orbital (9a″) (19% N_{calc}). In contrast, in **1** the Cu−N antibonding interaction in the S pπ bonding orbital is much weaker as judged by its reduced nitrogen character.[74] Figure 10 indicates that in **2**, the N character in both the S pπ bonding MO and the HOMO involves σ-type antibonding interactions between the 5b2 derived β-diketiminate orbital and the Cu $d_{x^2-y^2}$. Since the intensity of a CT band largely derives from overlap of the ligand orbitals in the ground and excited state and there is substantial overlap of the N-ligand orbitals in **2** in the S pπ − Cu $d_{x^2-y^2}$ bonding and antibonding (HOMO) orbitals, the N character will contribute additional intensity to the S pπ → Cu CT transition.

Time domain analysis of the RREPs (vide supra) gives a quantitative estimate for the S pπ → Cu CT excited-state distortion for the Cu−S bond ($\Delta_{\mathrm{ES}}(r_{\mathrm{Cu-S}})$) in **2** relative to **1** that is consistent with the above analysis of nitrogen-derived intensity in the S pπ → Cu CT band in **2** but not **1**: for **2** $\Delta_{\mathrm{ES}}(r_{\mathrm{Cu-S}}) \approx 0.12$ Å in comparison to **1** where $\Delta_{\mathrm{ES}}(r_{\mathrm{Cu-S}}) \approx 0.20$ Å.[20] In **1**, the large Cu−S distortion results from the strong S pπ character in the HOMO. This interaction is substantially reduced in **2**, due to a *trans* influence resulting from the strong β-diketiminate ligand contributions to the S pπ bonding orbital and antibonding orbital (i.e., HOMO). The reduced Cu−S character in these orbitals in **2** is consistent with its reduced excited-state distortion, because the change in the Cu−S bonding associated with the CT transition is smaller in **2** than in **1**. There is not a large distortion of the Cu−N bond since this interaction is antibonding in both the donor and acceptor orbitals.

Finally, the intense S pπ → Cu CT band in **2** (band 3) is shifted to 2500 cm^{-1} lower energy than the analogous band in **1**. In addition to the loss of the axial ligand, this reflects the high donor strength of the β-diketiminate ligand. There are three contributions to the reduced splitting between the S pπ bonding and antibonding (i.e., HOMO) orbitals, which determines the energy of the S pπ → Cu CT transition, in **2** relative to **1**. First, S K-edge XAS measurements suggest that there is substantially less S p character in the HOMO of **2** (32% S) than in the HOMO of **1** (52% S) due to the *trans* influence, which involves the observed decrease in the S pπ interaction with $d_{x^2-y^2}$ relative to **1**. This reduces the splitting of the S pπ bonding−antibonding pair, which reduces the energy of this CT transition. The second factor relates to differences in the antibonding N character in the S pπ bonding orbital (~20% N_{calc} in **2** vs ~12% N_{calc} in **1**, Figure 10B, but see footnote 74) This places the S pπ bonding orbital to less deep binding energy than its counterpart in **1** and contributes to a decreased S pπ CT transition energy in **2** relative to **1**. Finally, differences in the Z_{eff} of Cu in **2** versus **1** due to the loss of the axial ligand that are derived from observed XAS edge shift patterns (vide supra) and calculations (vide infra), influence this S pπ CT energy. The experimental shifts in the Cu L- and S K− preedge features indicate that three-coordinate complex **2** has a higher Z_{eff} than four-coordinate **1**. This places the d-orbital manifold (including the $d_{x^2-y^2}$ HOMO) to deeper binding energy which can contribute to a decrease in the S pπ CT energy, though this could be partially offset by the increased ligand field of **2** relative to **1**.

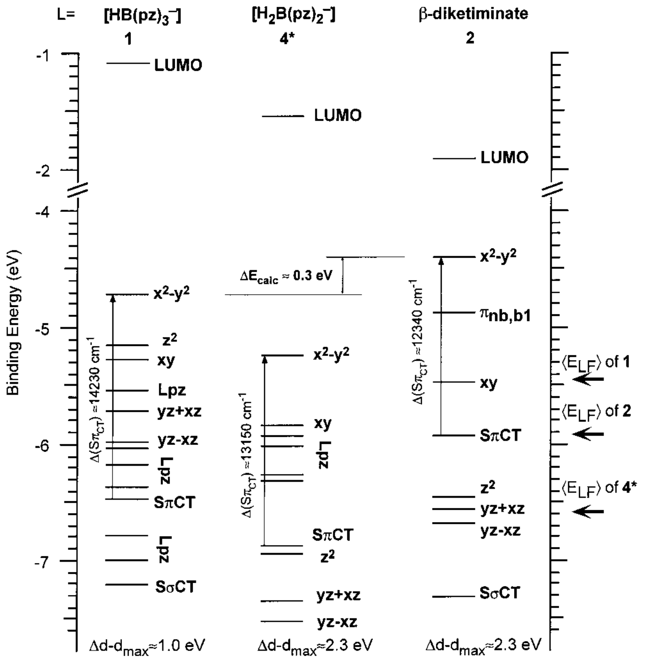

Figure 11. Calculated valence energy level diagrams showing electronic structural changes upon converting from [HB(pz)$_3$]CuSMe **1** → [H$_2$B(pz)$_2$]CuSMe **4*** → [$H_5C_3N_2$]CuSMe **2**. The bold, horizontal arrows on the right axis represent the average of the d-orbital energies, $\langle E_{\mathrm{LF}} \rangle$. For complexes **1**, **2**, and **4*** in order of decreasing binding energy (i.e., increasing Cu Z_{eff}) these values are −5.47, −5.92, −6.59 eV, sequentially.

3.6.4. Axial Ligand Effects. There are significant experimental and theoretical differences between the electronic structures of **1** and **2** (vide supra). It is possible to isolate the origins of these differences (vide supra) by systematically altering the geometry of **1** into **2**. First the axial ligand is removed to give **4***, a hypothetical trigonal bis(pyrazolyl)hydroborate ligated Cu thiolate. Next, the N-donor is changed from pyrazole to β-diketiminate (i.e., complex **2**). The effects of these geometrical changes on the energies of the valence orbitals are summarized in Figure 11.

Removing the axial ligand of **1** to generate the hypothetical planar, three-coordinate complex **4*** greatly increases the ligand field splitting, which is rather small in **1** due to its more tetrahedral geometry ($\Delta dd_{\mathrm{max}} = 8000$ cm^{-1} in **1** vs 18400 cm^{-1} in **4***). Further, in **4*** the S pπ bonding orbital is calculated to lie in the middle of the ligand field manifold. Both of these trends are analogous to those observed experimentally when comparing **1** to **2**, demonstrating the importance of the axial ligand. However, further electronic structural changes occur as the equatorial nitrogen ligand is changed from two pyrazoles in **4*** to β-diketiminate in **2**. Specifically, the one-electron energy difference of the HOMO and Spπ bonding orbitals (an approximation to the S pπ → Cu CT transition energy) is calculated to be ~1000 cm^{-1} higher in energy in **4*** than in **2**. This is partly due to a larger splitting of the Spπ bonding and antibonding orbitals as reflected by increased S pπ character in the HOMO of **4*** (48% S_{calc}). It also results from destabilization of the Spπ bonding orbital in **2** due to its substantial Cu−N antibonding character.

---

[74] In complex **1** the N-ligand does interact with the S pπ bonding orbital. However, this interaction involves N π orbital character that is orthogonal to that in the HOMO. Therefore, there is little ligand−ligand orbital overlap between the nitrogen contribution to the HOMO and Cu Spπ bonding orbital in **1**, and the N-ligand does not contribute to the intensity of a CT transition between these donor and acceptor orbitals.

Further, the HOMO of **4*** is calculated to lie 0.85 eV to deeper binding energy than the HOMO of **2**. This HOMO shift derives from a decreased effective nuclear charge in **2** relative to **4*** due to more efficient charge donation to the Cu from the β-diketiminate ligand relative to the bidentate bis(pyrazolyl)-hydroborate ligand. The horizontal arrows on the right ordinate in Figure 11 show the average energy of the entire d-manifold. These arrows indicate that in **4*** relative to **1** the entire d-block shifts to 0.85 eV deeper energy, which reflects a more positive Z_{eff} for Cu in **4*** due to the loss of the fourth (axial) ligand. Maintaining the three-coordinate trigonal geometry, but changing the equatorial ligand from bis(pyrazolyl)hydroborate to β-diketiminate, leads to an increase of the average d-block energy that reflects the strong donor strength of the latter ligand system relative to the former. However, the magnitude of the influence of the (fourth) axial ligand on Z_{eff} appears to be larger than that of the equatorial ligand.

Thus, both axial and equatorial ligand effects modulate the electronic structure of **1** versus **2**. The absence of an axial ligand in **4*** and **2** increases the LF splitting. The red shift of the Spπ CT band in **2** relative to **1** results from increases in Z_{eff} coupled with strong β-diketiminate ligation that leads to reduced S pπ bonding−antibonding splitting and a strong N−Cu antibonding interaction in the S pπ bonding orbital. The nature of the equatorial ligand is important because its donor strength can modulate the strength of the Spπ interaction which in turn can influence the magnitude of the S pπ bonding−antibonding splitting, and therefore the energy of the S pπ → Cu CT transition. In passing, we note that the calculations predict that the HOMO of **2** lies 0.3 eV above that of **1** due to the opposing influences from the relative ligand fields and the Z_{eff} values of the two compounds. This agrees reasonably well with the 0.2 eV shift to higher energy observed for the preedge feature in the S K-edge XAS experiment. This shift in **2** results from the partial cancellation of the stabilization of the d-manifold due to the increased Z_{eff}, by the larger ligand field splitting of the d orbitals of **2** relative to **1**.

4. Discussion

Although complexes **1** and **2** use the same strongly bonding triphenylmethylthiolate ligand, the loss of the axial ligand in **2** relative to **1** and differences in the bonding with the nitrogen ligands, tris(pyrazolyl)hydroborate in **1** and β-diketiminate in **2**, impart these two complexes with differences in their electronic structures. Geometrically, **2** is approximately trigonal planar,[19] while **1** is approximately trigonally distorted tetrahedral.[20,25,62] This geometric difference manifests itself by presenting the Cu(II) ion with different ligand fields that can be probed with MCD spectroscopy. The d → d bands in **2** are to significantly higher energy (>8000 cm^{-1}) than in **1**, which suggests that the trigonal geometry, and the β-diketiminate ligand associated with **2**, provides a stronger ligand field than in **1**. Another manifestation of the electronic structural differences of these compounds is the altered spectral characteristics of the S pπ → Cu CT transition of **2** relative to **1**: it shifts to lower energy, has reduced oscillator strength, and exhibits a smaller Cu−S excited-state distortion. The intensities of the XAS preedge features at the S K- and Cu L-edge regions point to Cu−S covalency in **1** and **2**, though there is less S p character in the HOMO of **2** than **1**. The ^{14}N superhyperfine coupling resolved in the EPR spectrum of **2** indicates that there is significant nitrogen character in its HOMO, which partially offsets the diminished S pπ interaction in this orbital. Further, the relative energy pattern of the S K-edge and Cu L-edge XAS features indicate that the effective nuclear charge of **2** is more positive than for **1**.

Scheme 2

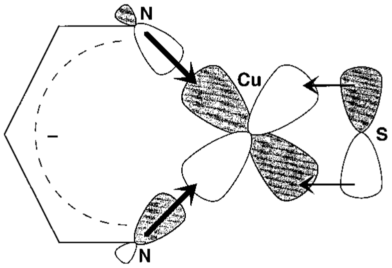

4.1. Nature of the β-Diketiminate: the *trans* Influence. The β-diketiminate ligand in **2** imparts this three-coordinate, trigonal complex with many of the unique aspects of its electronic structure relative to four-coordinate, distorted tetrahedral complex **1**. The negative charge of the β-diketiminate ligand in **2** is localized on the planar [C_3N_2] unit. The resulting destabilization of the orbitals of this anionic ligand is illustrated by a high energy orbital, 5b2 (Figure 8), which has virtually all of its wave function character on the nitrogen atoms. There is a strong σ-type donation from this 5b2 ligand orbital into the Cu d$_{x^2-y^2}$ orbital, with which it has the appropriate phase to interact. The strength of this interaction is reflected in the substantial ^{14}N superhyperfine observed in the EPR spectrum. As depicted in Scheme 2, this leads to a *trans* influence where the strong, in-plane interaction from the β-diketiminate ligand donates considerable electron density to the Cu d$_{x^2-y^2}$ at the expense of the thiolate S pπ interaction with this orbital. This *trans* influence is manifested in both the bonding and the antibonding S pπ − Cu d$_{x^2-y^2}$ combinations and leads to the observed differences between the S pπ → Cu CT transition in the absorption spectrum of **1** versus **2**, including its lower energy, lower oscillator strength, and smaller excited-state distortion. Further, this *trans* influence leads to the diminished S p covalency in the HOMO observed with S K-edge XAS.

4.2. Nature of the Cu−S Interaction. This *trans* influence of the β-diketiminate ligand suggests that the thiolate bond should be weaker in **2** than in **1**. Raman spectroscopy, which provides an experimental measure of the strength of the Cu−S bond through the stretching frequency, indicates that this expectation is not experimentally substantiated and that the Cu−S bonds in the two compounds have rather similar overall strengths, with **2** even slightly higher: ν(Cu−S) for **1** is 421 cm^{-1}, while ν(Cu−S) for **2** is 428 cm^{-1}. The similar S K-edge energies from the XAS measurements confirm that the net donor strength of S(thiolate) is similar in the two complexes. Calculations indicate that concomitant with the decrease in S pπ character in the HOMO of **2** due to the *trans* influence, there is a net increase in the Cu 4s and 4p mixing over the orbitals that are involved in the S pπ and S p pseudo-σ bonding interactions. These reflect donor interactions into the Cu 4s and 4p orbitals that can compensate for the reduced S pπ character in the HOMO and lead to comparable net Cu−S interactions. Thus, the total Cu−S bonding is similar in **1** and **2**, but the nature of these bonding interactions is different.

4.3. Role of the Axial Ligand. The fact that the net donation of the thiolate ligand in **2** is sufficient to give it a slightly stronger Cu−S bond than in **1** (as revealed by the increase in ν(Cu−S) from Raman) indicates the importance of the axial ligand, or its absence, in tuning the electronic structure of these molecules. For Cu thiolate systems without axial ligands, such as **2** and fungal laccase, it has been proposed that the thiolate can partially charge compensate for the missing axial ligand,[15] which leads to the stronger Cu−S interactions that are observed for these systems. The absence of an axial ligand in **2** also increases the importance of the equatorial nitrogen ligands, strengthening the donor interaction of the β-diketiminate ligand with Cu $d_{x^2\text{-}y^2}$. In this respect, the magnitude of the *trans* influence in **2** is a direct consequence of its trigonal (i.e., no axial ligand) geometry.

The edge and preedge energies in the S and Cu XAS experiments indicate a more positive Z_{eff} for **2** than **1**. Thus, in three-coordinate complex **2** the d-orbital manifold is stabilized relative to four-coordinate **1**. This demonstrates that the axial ligand plays a role in modulating Z_{eff} through its additional donor interaction with the Cu. Calculations confirm this, whereupon removing the axial ligand of four coordinate $[\text{HB(pz)}_3]\text{CuSR}_3$ **1** to give hypothetical three coordinate $[\text{H}_2\text{B(pz)}_2]\text{CuSR}_3$, **4***, the d-manifold moves to substantially deeper binding energy (arrows in Figure 11). Consistent with the XAS experimental results, the calculations on **1** and **2** give a similar trend though they involve different N-ligands (arrows in Figure 11). Relative to complex **2**, these theoretical results further indicate that hypothetical complex **4*** has a higher Z_{eff}, which confirms that the β-diketiminate ligand is a more strongly donating bidentate ligand than two pyrazoles, consistent with a substantial *trans* influence.

The axial ligand can also affect the overall ligand field. Our previously reported data for the blue Cu center in fungal laccase[15] and the calculations in Figure 11 indicate that the absence of an axial ligand leads to an increase in the energy of the d−d bands. This effect has been attributed to stronger in-plane ligand donor interactions. In trigonal planar complex **2**, this same effect appears to be operative and, along with strong N-donor interactions, is responsible for driving the ligand field transitions to exceedingly high energy.[75]

4.4. Comparison to Fungal Laccase. Since **2** is a good structural model complex for the blue Cu site in fungal laccase, it is important to compare the spectroscopic features of these two approximately trigonal Cu(II)−thiolate centers. The HOMO in fungal laccase bears a similar overall appearance to the HOMO of **2** in that they both exhibit a highly covalent interaction between the Cu $d_{x^2-y^2}$ and S pπ orbitals.[15] Yet, there are significant differences in their respective electronic structures. First, EPR measurements[19] indicate that there is substantially more nitrogen character in the HOMO of **2** than in fungal laccase. This compensates for reduced S 3pπ character in the HOMO of **2**.

The results for both fungal laccase and complex **2** indicate the importance of the axial ligand in modulating the strength of the ligand field. Upon changing from the prototypical blue Cu site in plastocyanin with an axial S(Met), to fungal laccase where this ligand is replaced by nonligating Phe or Leu to give a trigonal Cu(II) center, the ligand field is shifted to higher energy. The effect is even more dramatic if tetrahedrally distorted stellacyanin, with an axial O(Gln) ligand,[13] is used as the reference state.[11] A similar effect is observed in the model complexes compared in this study: upon removing the axial pyrazole ligand from **1**, the ligand field in trigonal **2** dramatically increases. Relative to fungal laccase, whose ligand field transitions are at high energy among blue Cu centers,[15] the ligand field transitions in **2** are at even higher energy (d_{yz-xz} at 20450 cm^{-1} in **2** versus 15600 cm^{-1} in fungal laccase). This reflects the donor strength of the β-diketiminate ligand relative to the analogous bis-imidazole ligand set in fungal laccase.

Comparison of the EPR properties of **2** ($g_{\|} = 2.169$, $g_{\perp} = 2.037$) to those of the blue Cu sites in fungal laccase ($g_{\|} = 2.201$, $g_{\perp} = 2.045$)[15] gives additional information about the relative strengths of the ligand fields of these two compounds. The ligand field expressions (eqs 3) relate the shifts in $g_{\|}$ and $g_{\perp}$ from the free electron value, $g_e = 2.0023$, ($\Delta g_q = g_q - g_e$, $q = \|, \perp$) to the energies of the ligand field transitions:

$$\Delta g_{\|}\,(\mathbf{2}) = \Delta g_{\|}\,(\text{laccase}) E_{xy}\,(\text{laccase})/E_{xy}\,(\mathbf{2}) \tag{3a}$$

$$\Delta g_{\perp}\,(\mathbf{2}) = \Delta g_{\perp}\,(\text{laccase}) E_{xz,yz}\,(\text{laccase})/E_{xz,yz}\,(\mathbf{2}) \tag{3b}$$

Here E_X represents experimentally determined d→d transition energies, where the average of the d_{yz+xz} and d_{yz-xz} energies are used for $E_{xz,yz}$. These equations give the values of 2.177 and 2.035 for $g_{\|}$ and $g_{\perp}$, respectively, which are in good agreement with the experimental values of **2**. Further, this analysis accurately predicts the decrease in $\Delta g_{\|}$ of 0.03 ($\approx 2.20 - 2.17$) for **2** relative to fungal laccase. This analysis demonstrates that the ligand field changes between fungal laccase and **2** are responsible for the changes in the g values. Likewise, the ^{63,65}Cu metal hyperfine interaction ($A_{\|}$), which is larger for **2** than for fungal laccase (-107×10^{-4} cm^{-1} vs -92×10^{-4} cm^{-1}), is scaled by the change in ligand field, as manifest in the relative $\Delta g_{\perp}$ and $\Delta g_{\|}$ values. Applying the ligand field relation: $A_{\|}(\mathbf{2}) \approx 396 \times 10^{-4}$ cm^{-1} $[[\Delta g_{\|}(\mathbf{2}) - \Delta g_{\|}(\text{laccase})] + {}^{3}/_{7}\,[\Delta g_{\perp}(\mathbf{2}) - \Delta g_{\perp}(\text{laccase})]] + A_{\|}(\text{laccase})$, gives an estimated $A_{\|}(\mathbf{2})$ of -106×10^{-4} cm^{-1}, in excellent agreement with experiment. Thus, the ligand field effects induced by the absence of an axial ligand, as discussed above, are also evident in the EPR spectral data.

Further, the S pπ → Cu CT transition in **2** shows reduced transition energy and intensity relative to the analogous band in fungal laccase at 600 nm. This energy shift of the CT band in **2** results from the strong interaction with the β-diketiminate ligand. Specifically, the combined influences of the reduced S pπ interaction and the destabilizing antibonding nature of the Cu−N interaction in the S pπ bonding orbital reduce the splitting of the S pπ bonding−antibonding pair, which together lead to the decreased CT energy. The band intensity can be described using the oscillator strength, which for the CT band in **2** ($f_{\text{exp,sc}}$(S pπ) is 0.066) is larger than in fungal laccase[15] (f_{exp}(S pπ) 0.055). This implies greater total ligand character in the HOMO of **2** relative to fungal laccase. However, this intensity increase in the S pπ → Cu CT band in **2** is not due to an increase in the thiolate covalency of **2** relative to fungal laccase. In fact, S K-edge XAS, which directly measures the S character in the HOMO, show less S character in **2** (32% S) than in plastocyanin (38% S). This latter value represents a lower limit for fungal laccase, since, based on the relative f_{exp}(S pπ) values[15] and ENDOR results,[68] the thiolate covalency in fungal laccase appears to be larger than in the prototypical blue Cu site in plastocyanin. These oscillator strength data can be understood based on differences in mixing in the S pπ bonding orbitals. In fungal laccase, this orbital is almost exclusively Cu−S pπ in character. In **2**, however, there is substantial (20% N_{calc}) Cu−N σ antibonding mixed into this level. The same Cu−N interaction is present in the HOMO of **2** and can contribute to the intensity of the low energy CT band since the ligand−ligand overlap from the N ligand orbital will be significant.

Finally, the MCD C-term signs in **2** are as observed in fungal laccase with the exception of the low-energy d_{z^2} transition (at

---

[75] From Figure 11, the loss of an axial ligand decreases the energy of the d_{z^2} orbital as observed experimentally (in **1**, the $z^2 \rightarrow x^2 - y^2$ transition (band 1) is at 5200 cm^{-1} while in **2** it is at 6300 cm^{-1}). The calculated change in energy is larger than that observed experimentally, which appears to be due to an overestimate in the 4s/d_{z^2} mixing in **2**.

6300 cm^{-1}), where this band exhibits positive sign in **2** but was negative in fungal laccase. The sign of an MCD band depends on the degree of ground- and excited-state spin−orbit coupling to different states.[76] The magnitude of this coupling depends inversely on the energy splitting between the d_{z^2} state and the ligand field or charge-transfer state that spin−orbit couples to it. Because, relative to fungal laccase, the ligand field states in **2** are at much higher energy, while the S p$\pi \rightarrow$ Cu CT state is at much lower energy, the degree of spin−orbit coupling between these states will be very different. In plastocyanin the sign of the $d_{z^2} \rightarrow$ HOMO transition is due to mixing of z polarization intensity associated with the Cu being displaced from the N_2S plane by ∼0.3 Å.[10,15] In fungal laccase the Cu is in this plane, and this mechanism for MCD intensity is eliminated, leading to the change in sign of the d_{z^2} transition.[15] In **2**, the Cu is displaced from of this plane by ∼0.2 Å,[19] which provides a spin−orbit mixing mechanism similar to plastocyanin. Thus, the observed out-of-plane shift of the Cu in **2** has electronic structural consequences.

In summary, for the two Cu(II) thiolate systems compared in this study, the absence of an axial ligand in **2** relative to **1** greatly contributes to the spectroscopic differences between the model complexes. The σ-donating bidentate β-diketiminate equatorial ligand in **2** also makes an important contribution to its electronic structure. Along with the loss of the axial ligand, these modifications contribute to the observed decrease in the S p$\pi \rightarrow$ Cu CT transition energy and the increase in the d → d transition energies. Further, relative to **1**, the stronger N-donor ligand in **2** changes its HOMO, through the increase in N covalency (as observed with EPR), and leads to a *trans* influence that decreases the thiolate covalency in the HOMO (as observed with S K-edge XAS). Although the β-diketiminate is a strong equatorial ligand, four-coordinate [3N + S] **1** has a lower Z_{eff} for Cu than three-coordinate [2N + S] **2**. The Raman spectra for **1** and **2** demonstrate that the total copper−thiolate bonding interactions in the two models are similar, which suggests compensation for the *trans* influence of β-diketiminate in the HOMO of **2** through thiolate bonding with Cu 4s and 4p orbitals. Thus, the loss of an axial ligand can modulate the electronic structure of blue Cu centers, through an increase in equatorial ligand donation. An increase in the covalency of the thiolate-Cu bond can affect the reorganization energy and increase electronic coupling into protein pathways for rapid electron transfer.

Acknowledgment. We thank Professor Thomas Brunold for the MathCAD script used for the time domain Raman analysis, Dr. Frank Neese for his EPR simulation program, as well as Professor Lawrence Que, Jr. and Dr. Raymond Y. N. Ho for access and assistance with resonance Raman spectroscopy at Minnesota. Financial support for this research program came from the NSF (CHE-9980546 to E.I.S.) and the NIH (GM-47365 to W.B.T.; RR-01209 to K.O.H.; GM-18812 to D.W.R.; GM-18991 to P.L.H.). SSRL operations are funded by the U.S. Department of Energy, Office of Basic Energy Sciences. The Structural Molecular Biology program at SSRL is supported by the National Institutes of Health, National Center for Research Resources, Biomedical Technology Program and by the Department of Energy, Office of Biological and Environmental Research.

Supporting Information Available: Table of Raman isotope shifts; figures showing: the rR spectrum of a second aryl thiolate complex $[HB(pz')_3]CuSC_6F_5$, the RREP for **3**, XAS spectra for the chloride starting materials of **1** and **2**, and input files for the calculations (PDF). An X-ray crystallographic report (CIF). This material is available free of charge via the Internet at http://pubs.acs.org.

JA001592O

---

[76] Neese, F.; Solomon, E. I. *Inorg. Chem.* **1999**, *38*, 1847−1865.